Acta Materialia 124 (2017) 633–659

Contents lists available at ScienceDirect

Acta Materialia

journal homepage: www.elsevier.com/locate/actamat

By invitation only: overview article

Ab initio modeling of dislocation core properties in metals and semiconductors

D. Rodney [a, *], L. Ventelon [b], E. Clouet [b], L. Pizzagalli [c], F. Willaime [d]

[a] Institut Lumière Matière, CNRS-Université Claude Bernard Lyon 1, F-69622 Villeurbanne, France
[b] DEN-Service de Recherches de Métallurgie Physique, CEA, Université Paris-Saclay, F-91191 Gif-sur-Yvette, France
[c] Institut Pprime, CNRS-Université de Poitiers, F-86962 Chasseneuil Futuroscope, France
[d] DEN-Département des Matériaux pour le Nucléaire, CEA, Université Paris-Saclay, F-91191 Gif-sur-Yvette, France

ARTICLE INFO

Article history:
Received 31 May 2016
Received in revised form
29 August 2016
Accepted 27 September 2016
Available online 21 October 2016

Keywords:
Dislocation
Plasticity
Alloys
Semiconductors
Density functional theory

ABSTRACT

Dislocation cores, the regions in the immediate vicinity of dislocation lines, control a number of properties such as dislocation mobility, cross-slip and short-range interactions with other defects. The quantitative modeling of dislocation cores requires an electronic-level description of atomic bonding. *Ab initio* quantum mechanical calculations of dislocation cores based on the density functional theory have progressed rapidly thanks to the steady increase in computing capacities and the development of dedicated numerical methods and codes. Our aim in this overview paper is, after a description of the methodology regarding in particular the boundary conditions, to review the new and unexpected results obtained on dislocation cores from first principles, including the identification of unforeseen stable and metastable cores and the quantitative evaluation of both interaction energies and energy pathways, in pure metals and alloys of different crystallography (FCC, BCC, HCP) as well as semiconductors. We also identify key challenges to be explored in this rapidly growing field.

Contents

* Corresponding author.
E-mail address: David.Rodney@univ-lyon1.fr (D. Rodney).

http://dx.doi.org/10.1016/j.actamat.2016.09.049
1359-6454/

1. Introduction

Crystal plasticity is an inherently multi-scale process starting at the atomic scale where dislocation cores, the regions in the immediate vicinity of dislocation lines, control a number of local properties, including the selection of glide planes and corresponding dislocation mobility, cross-slip and nucleation processes [1–5].

While the elasticity theory of dislocations [6–8] describes very accurately the long-range stress and strain fields produced by dislocations, an atomic-scale description is required to describe reconstructed regions like dislocation cores. Historically, the first model of a dislocation core involved an elasto-plastic framework, the well-known Peierls-Nabarro model [9,10], where the atomic-scale description was limited to the dislocation glide plane. Later, full atomistic calculations of dislocation cores [11] were performed using interatomic short-ranged pair potentials, almost simultaneously in face-centered cubic (FCC) [12–14] and body-centered cubic (BCC) metals [15,16]. Since then, empirical and semi-empirical potentials have been applied to a very large variety of dislocations in metals and alloys, intermetallic compounds, semiconductors as well as covalent and ionic crystals (seminal works include Refs. [17–24]). Interatomic potentials are very useful to study large-scale processes at finite temperatures, but they remain of limited predictability regarding the detailed structure of a dislocation core. A famous example is the long-term debate about the core structure of screw dislocations in BCC metals, which is predicted by interatomic potentials in two different forms, symmetrical and asymmetrical, depending on the details of the potential parameters [23,25–28].

To be quantitative and predictive, an electronic-level description of atomic bonding is required, as provided by *ab initio* quantum mechanical calculations performed within the density functional theory (DFT) [29]. The first calculations of a dislocation core concerned semiconductors [30–32], partly because electronic structure calculations in semiconductors require less computing resources than in metals. However, metals were soon considered: BCC [33], hexagonal close-packed (HCP) [34,35] and finally FCC [36]. Initially limited to pure metals, current studies also consider alloying effects.

Ab initio calculations are very computationally demanding and allow to simulate only a few hundreds of atoms. As a result, the calculations are mainly limited to straight infinite periodic dislocations. But even then, the lateral dimensions do not exceed a few nanometers, such that, given the long-range stress and strain fields produced by a dislocation, interactions with the boundary conditions are inevitable. These interactions affect the dislocation energy and possibly even its core structure. Therefore, *ab initio* calculations of dislocations, more than any other defect or simulation method, require a very careful choice of the boundary conditions. Fortunately, a large effort has been devoted this past decade to either develop adapted boundary conditions [37–39] or control and remove boundary condition effects, notably their elastic contribution [40,41].

Ab initio calculations of dislocation cores have recently made very rapid progress, because of the combined increase in computing power, progress in methodology particularly regarding boundary conditions and progress in scientific computing through the development of efficient workpackages like the Vienna Ab initio Simulation Package (VASP) [42], the PWSCF package, which is part of the QUANTUM ESPRESSO integrated suite of codes [43], and the SIESTA [44] and ABINIT [45] packages.

Our aim in this overview is to highlight the unique input *ab initio* calculations have brought to the modeling of dislocation cores and identify the outstanding challenges that remain in this rapidly growing field. After a description of the methodology (Sec. 2), we will consider the modeling and understanding of dislocation core properties in both metals and semiconductors. We will start with FCC metals (Sec. 3) where cores are probably the simplest but remain challenging for *ab initio* calculations because of their large dissociation. We will then address BCC metals (Sec. 4), where cores are more compact but show an intricate relation with the crystallography and applied stress. Following, we will consider HCP metals (Sec. 5), where several metastable cores have recently been identified. Finally, we will address semiconductors (Sec. 6), where the existence of the shuffle and glide systems, as well as charge effects in compound elements, induce a large variety of cores with complex structures.

2. Methodology

We start this overview by considering methodological aspects related to dislocation modeling. We first present generalized stacking fault energy (GSFE) calculations, an instructive first step towards the study of dislocation cores. We then describe three classes of boundary conditions used for *ab initio* dislocation modeling, insisting on their differences and respective advantages and drawbacks. We end with details of DFT calculations important to model defects in crystals.

2.1. Generalized stacking fault energies

Dislocation core structures and mobilities are partly controlled by the ease to shear a crystal along a given crystallographic plane, which can be characterized by a generalized stacking fault energy surface [46,4], also called a γ-surface. In these calculations, a crystal is cut along a fault plane and the resulting half-crystals are shifted by a fault vector $\boldsymbol{\gamma}$ belonging to the fault plane (Fig. 1). Atoms are then relaxed in the direction perpendicular to the fault plane to obtain the γ-surface, *i.e.* the 2D fault energy as a function of fault vector. Note however that this vertical relaxation is not necessary when the GSF is defined as a 3D function and is used to parameterize the Peierls-Nabarro model [47]. Note also that the same calculations can be generalized to multiplane faults as proposed in Ref. [48].

Local minima on the γ-surface correspond to stable stacking faults responsible for the splitting of perfect dislocations into partial dislocations, as in FCC (see Sec. 3) and HCP (see Sec. 5) crystals. However, one needs to check that the stacking fault remains stable once the atoms are allowed to relax in all directions. Even when no minimum is found, γ-surfaces still provide useful information about the planes and associated directions that can be easily sheared. γ-surfaces thus serve as a first step to discriminate between different potential glide systems. Finally, γ-surfaces are used as input parameters in elasto-plastic models like the Peierls-Nabarro model [9,10,49–51] (see Sec. 3).

Different boundary conditions can be used to compute generalized stacking faults. In the directions defining the fault plane, periodicity is enforced to simulate an infinite fault. In the perpendicular direction, one can use either free surfaces (Fig. 1a) or periodic boundary conditions provided a shift equal to the fault vector is added to the out-of-plane periodicity vector (Fig. 1b). Full periodic boundary conditions should be preferred because they maximize the distance between planar defects, and thus minimize their interactions. Moreover, the introduction of surfaces induces a discontinuity in the electronic density, which slows down the convergence of the electronic self-consistency, and induces oscillations in the fault energy as a function of simulation cell height [52].

Because relaxations are allowed only perpendicularly to the fault plane, stable stacking faults may be missed on a γ-surface. An example is the second order $\{\bar{2}11\bar{2}\}$ pyramidal plane in HCP metals [53], where no relevant minimum is found for the splitting of $\langle c+a\rangle$ dislocations (see Sec. 5) when only perpendicular relaxations are allowed. However, a minimum does appears when all atoms, except those just above and below the fault plane, are allowed to fully relax. Note that the nudged elastic band (NEB) method [54] can also be used to obtain such relaxed γ-lines [55]. This sensitivity of the γ-surface on the way atomic positions are relaxed is even more important in more complex crystalline structures with several atoms per primitive unit cell. An example is Fe_3C cementite [56].

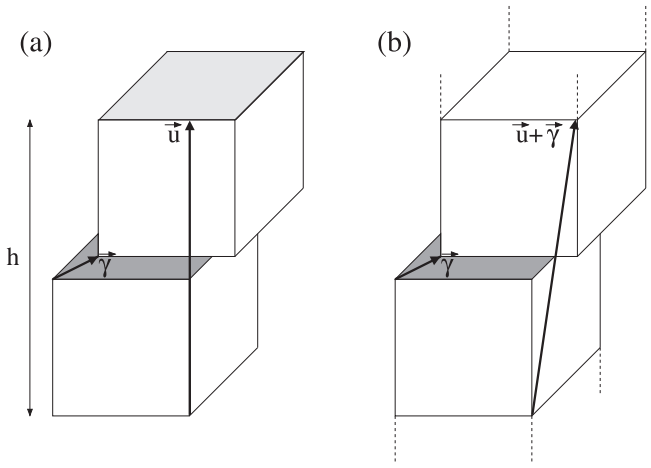

Fig. 1. Boundary conditions to calculate generalized stacking fault energies: (a) free surfaces, (b) periodic boundary conditions.

2.2. Dislocations and boundary conditions

The boundary conditions to model dislocations have to be chosen with care because dislocations produce long-range elastic fields and are thus sensitive to the boundary conditions at long distances. Also, a single dislocation cannot be introduced in a simulation cell with full periodic boundary conditions, which usually constitutes the paradigm to model bulk materials: a dislocation creates a displacement discontinuity that has to be closed by another defect to allow for periodicity. As a result, different boundary conditions have been developed.

2.2.1. Cluster approach

The easiest way to model a straight dislocation is to use a cylinder with an axis parallel to the dislocation line along which periodicity is enforced. The dislocation is created by displacing all atoms according to the Volterra solution given by anisotropic elasticity [6,7,57,58]. Atoms on the cylinder surface (region 2 in Fig. 2a) are then kept fixed at their initial position while the atoms inside the cylinder are relaxed.

One caveat with this approach is that the Volterra elastic solution yields only the long-range elastic field of the dislocation. Close to the dislocation line, an additional contribution, the dislocation core field, needs to be accounted for [59]. A spreading of the dislocation core produces such a core field, but even dislocations with a compact core, like $1/2\langle 111\rangle$ screw dislocations in BCC metals, possess a non-negligible core field [60]. Rigid boundary

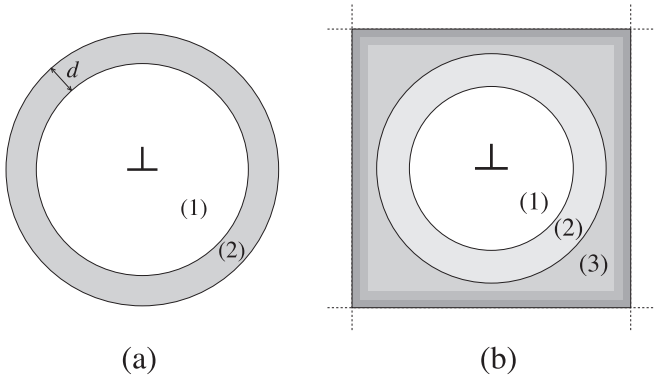

Fig. 2. Cluster approach to model an isolated straight dislocation. The outer boundary is either (a) rigid or (b) flexible and controlled by lattice Green's functions or by coupling to an empirical potential.

conditions do not allow for a full development of the core field, which, although decaying more rapidly than the Volterra field, may still affect the relaxation of the dislocation core.

Also, with this approach, calculations of the Peierls stress, which corresponds to the stress above which the dislocation starts to glide without the help of thermal fluctuations, must be corrected to account for the fact that when the dislocation moves, the boundary conditions are no longer compatible with the dislocation position. The resulting back stress may however be computed and corrected from the Peierls stress calculation [61,62].

Finally, similarly to the GSFE calculations, the presence of vacuum results in numerical inefficiencies with *ab initio* codes based on plane waves, like VASP and PWSCF. Also, the discontinuity of the electronic density induces oscillations in metals that may affect the core properties [29].

2.2.2. Flexible boundary conditions

To avoid some of the artifacts induced by rigid boundary conditions, flexible boundary conditions have been developed, based either on a lattice Green's function [63] or on a coupling with an empirical potential [39,64].

The lattice Green's function $G_{ij}(\vec{r})$ expresses in an harmonic approximation the displacement $\vec{u}$ induced on an atom at position $\vec{r}$ by a force $\vec{F}$ acting on an atom at the origin:

$$u_i(\vec{r}) = \sum_j G_{ij}(\vec{r}) F_j. \quad (1)$$

The lattice Green's function can be obtained by inverting the force-constant matrix of the perfect crystal [65–67] or can be tabulated from direct calculations [37,63,68,69].

Three zones are now defined (Fig. 2b). Atoms in the inner zone 1 are relaxed with *ab initio* forces, keeping fixed atoms in zones 2 and 3. The resulting atomic forces in zone 2 are then relaxed using the lattice Green's function in Eq. (1) to displace the atoms in all three zones. This process is repeated iteratively until all forces in zones 1 and 2 are below a threshold. Atoms in zone 3 serve as a buffer to prevent forces in zone 2 to be influenced by the external boundary. Zone 3 may be cylindrical as with rigid boundary conditions, but this region may need to be quite large in metals to minimize perturbations in the inner regions [70]. Alternatively, zone 3 can be surrounded by periodic boundaries [29]. Surface defects or dislocations then form at the boundary but they are not explicitly included in the force calculations and perturb less the electronic density than vacuum. This solution is also numerically advantageous with plane-wave DFT codes as mentioned above and can be used in the cluster approach as well.

The lattice Green's function is less straightforward to implement than rigid boundary conditions but it allows to take full account of the dislocation core fields [36,37,69] (for an implementation in VASP, see Ref. [71]). These boundary conditions also adapt under an applied deformation, allowing to determine the core configuration under finite stresses and to calculate the Peierls stress [69].

Another approach relies on coupling the *ab initio* calculations with an empirical potential, a so-called Quantum Mechanical/Molecular Mechanics, or QM/MM, coupling [39,64,72]. The simulation box is still divided in 3 regions (Fig. 2b). *Ab initio* calculations are performed only in regions 1 and 2. Atoms in regions 2 and 3 are relaxed according to the forces calculated with an empirical potential, whereas atoms in region 1 are relaxed according to *ab initio* forces plus a correction to withdraw the perturbation caused by the coupling outside the *ab initio* region. The buffer region 2 was added to minimize this correction. To operate, this method needs an empirical potential that matches as best as possible the *ab initio* calculations, at least the lattice constants and elastic moduli, but also preferably the full harmonic response. This concurrent multiscale approach can be further developed to couple the region described with the empirical potential to a larger region where continuum mechanics is used to apply complex loading [38].

The main drawback of the flexible boundary conditions is the difficulty to extract dislocation energies. Because of the energy formulation inherent to *ab initio* calculations, one cannot easily partition the excess energy between the dislocation and external boundary contributions, although methods to project the energy on atoms have been proposed [73]. It is thus possible to calculate, for instance, the Peierls stress, but not the Peierls energy.

2.2.3. Periodic boundary conditions

To avoid external boundaries and use periodic boundary conditions in all three directions, a dislocation dipole, *i.e.* two dislocations with opposite Burgers vectors, must be introduced in the simulation cell. A 2D periodic array of dislocations with alternating Burgers vectors is then modeled (Fig. 3).

Several inequivalent arrays can be devised, but quadrupolar arrangements should in most cases be preferred because they minimize the Peach-Koehler force due to image dislocations [32,40,41,60,74,75]. A periodic array is quadrupolar if there exist periodicity vectors, $\vec{U}_1$ and $\vec{U}_2$, for which the vector linking the two dislocations of the dipole is equal to $1/2\,(\vec{U}_1 + \vec{U}_2)$ (Fig. 3). This ensures that every dislocation is a center of symmetry in the array, meaning that if there is a dislocation with Burgers vector $\vec{b}$ at position $\vec{r}$ with respect to a given reference dislocation, there is also a dislocation $\vec{b}$ at $-\vec{r}$, such that the stress created by both dislocations cancels to first order at the reference dislocation, thanks to the symmetries of the Volterra elastic field [6].

Linear elasticity is still used to build the initial configuration, making sure that the cut surface, defined by the cut vector $\vec{A}$ (Fig. 3), lies in-between the two dislocations of the dipole. All atoms are displaced according to the superposition of the displacement fields created by each dislocation of the periodic array, with the summation performed either in reciprocal space [75,76] or in direct space after regularization of the conditionally convergent sums [40,41]. Also a homogeneous strain needs to be applied to the simulation cell to accommodate the plastic strain created by the dipole [40,41,75,76]. This can be easily demonstrated by considering the variation of elastic energy when a homogeneous strain ε_{ij} is applied to a simulation cell containing a dislocation dipole with Burgers vector $\vec{b}$ and cut vector $\vec{A}$ [60]:

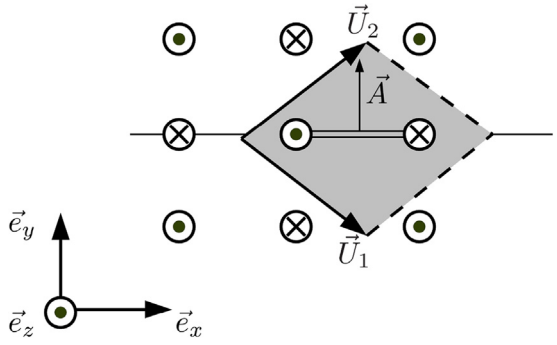

Fig. 3. Dislocation dipole with periodic boundary conditions. The dipole is defined by its Burgers vector $\vec{b}$ and cut vector $\vec{A}$. $\vec{U}_1$ and $\vec{U}_2$ are periodicity vectors of the simulation cell.

$$\Delta E(\varepsilon) = h\left(\frac{1}{2}SC_{ijkl}\varepsilon_{ij}\varepsilon_{kl} + C_{ijkl}b_iA_j\varepsilon_{kl}\right),$$

where S is the area of the simulation cell perpendicular to the dislocation line, h the corresponding height, and C_{ijkl} the elastic constants. The average stress in the simulation cell is then

$$\sigma_{ij} = \frac{1}{hS}\frac{\partial \Delta E}{\partial \varepsilon_{ij}} = C_{ijkl}\left(\varepsilon_{kl} - \varepsilon^0_{kl}\right), \quad (2)$$

with the plastic strain

$$\varepsilon^0_{kl} = -\frac{b_kA_l - b_lA_k}{2S}. \quad (3)$$

One can see that the stress in Eq. (2) is zero when the applied strain ε_{ij} is equal to the plastic strain ε^0_{ij}. Otherwise, a Peach-Koehler force acts on the dislocations, which can be used to study them under an applied stress and for instance determine their Peierls stress. Finally, when a stress variation is observed during a simulation, Eq. (2) allows to deduce the corresponding plastic strain increment, and through the cut vector $\vec{A}$ in Eq. (3), the change of relative position between dislocations. This has been used to define dislocation positions [77,78].

The main advantage of periodic boundary conditions is to yield a well-defined energy. However, in order to isolate the dislocation core energy, the DFT energy must be corrected to remove the interaction between the dislocations of the dipole and between these dislocations and their periodic images. If linear elasticity is assumed, the correction can be computed, considering the Volterra elastic field created by the dislocations calculated either in reciprocal [75,76] or direct space [40,41]. Because of the small size of the simulation cells, it may also be necessary to include the dislocation core fields [60,79,80]. For dissociated dislocations, the elastic interaction between dislocations can affect the dissociation distance, and hence the associated dislocation energy, but this can again be modeled within linear elasticity to recover the energy of an isolated dissociated dislocation [75].

Of particular interest is the Peierls energy, *i.e.* the energy barrier opposing dislocation glide. This barrier is the minimum energy path when a dislocation changes Peierls valley, which can be calculated using either a simple constrained minimization algorithm or the NEB method [54]. If one dislocation of the dipole is displaced keeping the second dislocation fixed, the relative distance between dislocations varies along the path and the elastic energy and stress (see Eqs. (2) and (3)) must be corrected [62,75,81,82]. Another option is to displace both dislocations simultaneously [83]. However, this is possible only if the path is symmetrical because the dislocations will traverse the Peierls valley in opposite directions. For instance, this solution cannot be used under an applied stress.

A final point is that calculations of the Peierls barrier give the variation of the dislocation core energy as a function of a reaction coordinate, which is different from the dislocation position. To fully characterize the Peierls potential and for instance estimate the Peierls stress, one needs to extract the dislocation position in each image of the path. Several methods have been proposed, based on a fit of the atomic disregistry with the Peierls-Nabarro model [83,84], on a fit of the atomic displacements with the Volterra solution [85,86], on the displacements of the core atoms [87], or on the stress variation when the dislocations move in opposite directions [77,78].

2.3. DFT technicalities

The choice of DFT approximations and parameterizations is crucial to accurately model dislocation core properties. One should keep in mind that the energy variations involved in dislocation glide are small, particularly in metals. For instance, the Peierls energy does not exceed 100 meV/b for the 1/2⟨111⟩ screw dislocation in BCC transition metals [88,82]. As a consequence, a strict criterion on atomic forces is needed during energy minimization.

The periodicity along the dislocation line allows to use a reduced length of the supercell to model a straight dislocation. Special care is recommended in choosing an adequate number of k-points along the line (for instance, typically 16 k-points per Burgers vector for BCC screw dislocations [81,82,85]).

The effects of the pseudopotential scheme and of the semicore electrons included in the valence states are usually not significant for dislocation modeling. For instance, the same shape of Peierls barrier is obtained for the 1/2⟨111⟩ screw dislocation in BCC Fe with an ultrasoft pseudopotential (USPP) [86] and the projected augmented wave (PAW) method [82] with only a slight variation of the barrier height (35 meV/b with USPP and 40 meV/b with PAW). There are however exceptions. For instance in Mg modeled with VASP, the prismatic configuration of the 1/3⟨1$\bar{2}$10⟩ screw dislocation was found unstable with USPP [89,90] and metastable with PAW [90,91] (see Sec. 5).

The effect of the exchange-correlation functional can be significantly more important depending on the system. Still in the case of the BCC screw dislocation, DFT calculations showed that the Peierls barrier obtained with two different exchange-correlation functionals, namely the Perdew-Burke-Ernzerhof generalized gradient approximation (GGA) [92] and the local density approximation (LDA), may differ by approximately 20% in Ta [88]. This effect is even more pronounced in Fe because of magnetism [86]. As shown in Fig. 4, both functionals lead to a single-hump Peierls barrier, but with a height 40% lower with LDA than GGA.

3. FCC metals

3.1. Generalized stacking fault energy

In FCC metals, the dislocations mainly responsible for plastic deformation have a 1/2⟨110⟩ Burgers vector and glide in dense {111} planes, where they are dissociated into a pair of Shockley partials with 1/6⟨112⟩ Burgers vectors, separated by an intrinsic

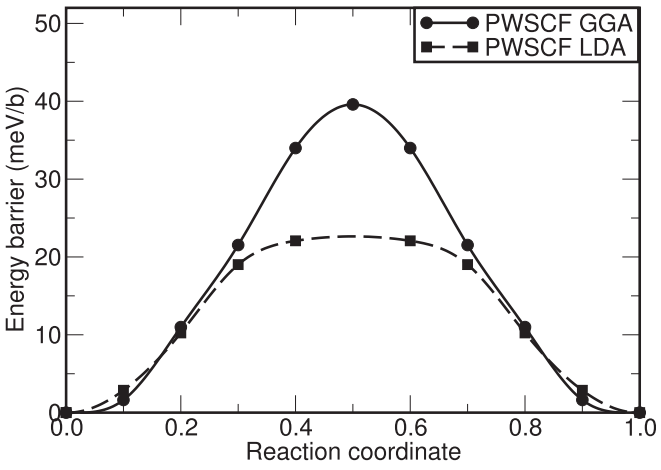

Fig. 4. Influence of the exchange-correlation functional on the Peierls barrier of the 1/2⟨111⟩ screw dislocation in BCC Fe. Adapted with permission from Ref. [86].

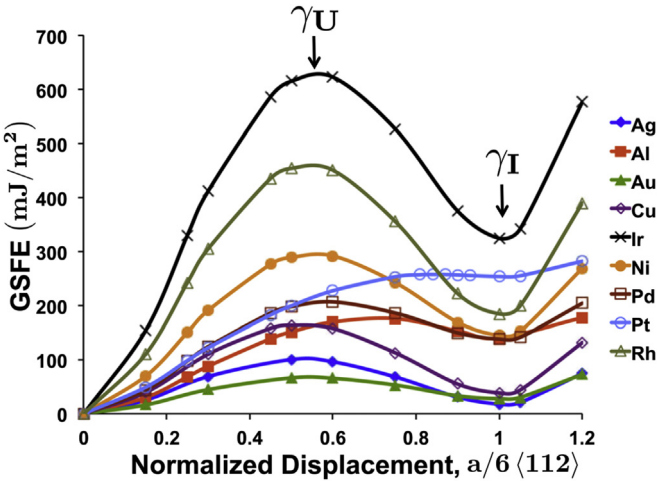

Fig. 5. Examples of γ-lines in {111} planes along a ⟨112⟩ direction in different FCC metals (VASP PAW GGA calculations). Reproduced with permission from Ref. [100].

stacking fault (ISF) where the atomic stacking is locally HCP [5,6,93]. As illustrated in this Section, although the FCC planar core is probably one of the simplest, its quantitative study, important to understand processes such as short-range interactions with other crystalline defects [94], cross-slip [95] or homogeneous [96] and inhomogeneous nucleation [97], remains challenging.

Dissociated dislocations have been modeled using interatomic potentials since the mid-1960's (see Refs. [13,14] for an early study, Ref. [98] for more recent calculations). However, most interatomic potentials underestimate the ISF energy [99] and consequently overestimate the dissociation distance. On the other hand, with the exception of Al, dissociation distances are too large in FCC metals to allow for direct calculations from first principles.

An alternative approach to include electron-based information is to employ elasto-plastic models, namely the Peierls-Nabarro and phase field models. A dislocated crystal is then described as two elastic continuum half-spaces connected along the dislocation glide plane by an interplanar potential, which corresponds to the GSFE. These models are well adapted to FCC dislocations because most of the atomistic effects occur in the glide plane where the dislocation dissociates.

All input for the elasto-plastic models, the lattice parameter, elastic constants and GSFE can be computed from first principles. For FCC metals, the relevant GSFE is parallel to a {111} plane. Examples of 1D cuts along the ⟨112⟩ direction are shown in Fig. 5 for several FCC metals. This direction contains both the so-called unstable stacking fault (USF), the saddle point of the GSFE, and the ISF, which corresponds to a local minimum. Note that the depth and curvature around the ISF vary widely from metal to metal.

Table 1 collects representative data with comparisons to experiments. The GSFE is represented by the USF (γ_{US}) and ISF energies (γ_{SF}). All data in Table 1 were obtained with VASP, using PAW pseudopotentials within the GGA approximation. The data are spread among authors, resulting from different choices of kinetic energy cut-off for the plane-wave basis set, of density of the k-point Monkhorst-Pack mesh and broadening width used to sample the Brillouin zone and of simulation cell size (these parameters are unfortunately not systematically mentioned in the publications). Al, Cu and Ni have attracted most of the attention, allowing for some statistics and showing that stacking faults are computed with a standard error of ~8%, which is actually small compared to experimental uncertainties.

3.2. Elasto-plastic models

PN and phase field models, parameterized on the GSFE, elastic constants and lattice parameters have been used to predict dislocation core structures, with the edge dislocation in Al as primary object of study (see Table 2). The dissociation distance is evaluated from the separation between maxima in the distribution of Burgers vector in the dissociation plane. The first calculations [109–111], based on the LDA approximation and a semidiscrete variational formulation of the PN model, found no or a very small dissociation of the edge dislocation in Al (3.5 Å). A larger dissociation (7.8 Å) was found using a generalized 2D PN model [112], while adding extra gradient terms to better represent the discreteness of the lattice [107] yielded even larger dissociations (10.3 Å). Using a phase field model, intermediate distances were found, 6.3 Å [113] and 5.7 Å [100]. Globally, the relative difference between elasto-plastic models of edge dislocations in Al is ~30%, highlighting the difficulty to model quantitatively even this relatively simple dislocation core. Comparison with experiments is also difficult, since two rather different dissociation lengths have been estimated, 8 Å from weak-beam TEM (WB-TEM) [114] and 5.8 Å from high-resolution TEM (HR-TEM) [115]. One difficulty in experiments is to avoid free surface effects that tend to rotate the partials towards their Burgers vector, thus closing the dissociation on one end and extending it on the other end [116].

The elasto-plastic models were used to systematically study the dependence of the stacking fault width on the GSFE surface in a number of FCC metals [100,107,117]. The results are reproduced in Fig. 6. We recover the general linear dependence of the dissociation distance on the adimensional ratio Gb/γ_{SF} (G is an equivalent

Table 1
Intrinsic and unstable stacking fault energies in FCC metals computed with VASP PAW GGA (in mJ m^{-2}). Experimental data between parenthesis are from Ref. [6]. Sources for DFT data are: [a] [48], [b] [101], [c] [102], [d] [36], [e] [103], [f] [104], [g] [105], [h] [106], [i] [107], [j] [108], [k] [100].

Metal	Stacking fault (mJ m^{-2})	
	Intrinsic γ_{SF}	Unstable γ_{US}
Ag	18[c,k], 17[f], 16[g] (16)	133[c],111[f], 91[g], 100[k]
Au	33[c], 27[f], 25[g], 28[k] (32)	134[c], 94[f], 68[g], 67[k]
Cu	41[c,e], 39[a,k], 43[f], 38[b], 43[i], 36[g] (45)	180[c,e], 158[a,g], 175[f], 164[b,k], 175[i]
Ni	110[c], 137[b], 133[g], 131[j], 142[f], 145[k] (125)	273[c], 278[b], 258[g], 305[j],289[k]
Al	130[c], 134[e], 158[a,i,f], 140[k], 146[b], 122[d], 162[h], 112[g] (166)	162[c], 169[e], 175[a], 140[g], 178[b], 225[i,f], 189[h], 177[k]
Pd	168[c], 122[i], 134[g], 138[k] (180)	287[c], 215[i], 202[g],198[k]
Pt	324[c], 282[i], 286[g], 254[k] (322)	339[c], 311[i], 286[g], 258[k]

Table 2
Dissociation distances for edge and screw dislocations in Al, estimated from experiments, elasto-plastic models and atomistic calculations.

Method	Edge (Å)	Screw (Å)
WB-TEM [114]	8.0	
HR-TEM [115]	5.8	
Semidiscrete PN [110]	3.5	2.1
Generalized PN [112]	7.8	
Gradient PN [107]	10.3	
Phase Field [113]	6.3	
Phase Field [100]	5.7	4.1
QC-DFT [38]	5.6	
QM/MM [39]	5.9	
FP-GFBC [36]	7.0	5.0
OF-DFT (LDA) [118]	13.7	7.4
OF-DFT (LDA) [119]	20.4	10.9
OF-DFT (LDA, Real space) [120]	12.8	

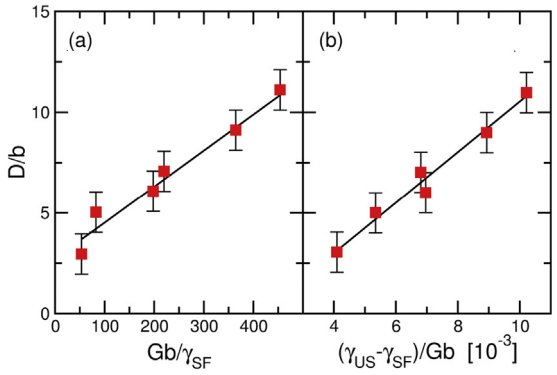

Fig. 6. Elasto-plastic modeling of FCC dislocations. Dependence of the scaled dissociation distance (D/b) of an edge dislocation on the adimensional parameter Gb/γ_{SF} ($G = (3C_{44}+C_{11}-C_{12})/5$ is an equivalent isotropic shear modulus) and on the scaled energy difference between unstable and stable stacking fault energies $(\gamma_{US}-\gamma_{SF})/Gb$ for 6 FCC metals (Al, Pd, Au, Ni, Cu and Ag in order of increasing D/b). Adapted with permission from Ref. [117].

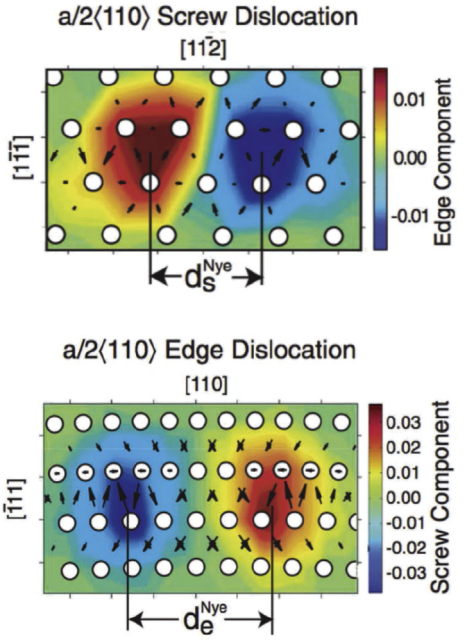

Fig. 7. Core structures of screw and edge dislocations in FCC Al predicted using DFT with lattice Green's function boundary conditions [36]. The color code depends on the local density of Burgers vector evaluated from the Nye tensor. The arrows show the corresponding differential displacement maps. Reproduced with permission from Ref. [36]. (For interpretation of the references to colour in this figure legend, the reader is referred to the web version of this article.)

isotropic shear modulus) expected from linear elasticity [6]. The balance reflected by this ratio between the elastic repulsion between partials and the energetic cost of the ISF still dominates, even though in the elasto-plastic models, the partials are spread and the plastic shear evolves across the stacking fault. Stacking fault widths may depend on other features than the GSFE. For instance, phase field simulations found a dependence on the difference $\gamma_{US}-\gamma_{SF}$ (see Fig. 6b), which reflects the curvature of the GSFE around the ISF [117,100].

3.3. Full atomistic calculations

Owing to their small dissociations, only edge and screw dislocations in Al have been modeled using full DFT calculations, and even then, in order to limit the effect of the boundary conditions, a coupling was needed to a larger system modeled either with an interatomic potential or lattice Green's functions. The first calculation used a quasicontinuum coupling (QC-DFT) [38] with an 84 atom DFT cell surrounded by a region modeled with an interatomic potential, predicting a 5.6 Å dissociation for the edge dislocation in Al. Adding a row of H atoms in the stacking fault was shown to increase the dissociation to 13 Å. Later, an improved QM/MM coupling was proposed [39], introducing a buffer of atoms between the DFT and interatomic potential regions where the energy is calculated with DFT but the forces with the interatomic potential. With 126 atoms in the DFT and buffer regions, a dissociation of 5.9 Å was found. However, calculations coupling the DFT region to a discrete elastic system using lattice Green's functions [36] (first principles lattice Green's function boundary conditions, FP-GFBC), with a 137 atom DFT region, found larger dissociation distances. The corresponding core structures for the edge and screw dislocations are shown in Fig. 7. Using the Nye tensor to identify the position of the Schockley partials, a dissociation of 7 Å was found. Finally, orbital-free DFT (OF-DFT), an efficient scheme to compute electronic structures in nearly-free-electron metals like Al, has been used in cells containing several thousand atoms in both periodic and cylindrical cells [118–120], resulting in rather large dissociations above 12 Å for the edge dislocation and 7 Å for the screw dislocation. Interestingly, this method [119] predicts a mestable non-dissociated core structure for the screw dislocation, which may play a role in the discrepancy between internal friction and mechanical deformation measurements of the Peierls stress of FCC dislocations [121].

Full DFT calculations confirm the general structure of the FCC planar core, but the spread in the predicted dissociation distances, which still seems affected by the limited size of the DFT region, does not yet allow for a fully quantitative evaluation of the dissociation length and its dependence on alloying elements.

4. BCC metals

4.1. The easy core configuration in pure metals

Plasticity in BCC metals at low temperatures is well known to differ substantially from closed-packed metals, like FCC metals seen in previous Section. Experimentally, low-temperature microstructures in BCC metals are dominated by screw dislocations with an $1/2\langle 111\rangle$ Burgers vector. Glide loops in {110} planes contain long straight screw segments due to their low mobility, with shorter and highly curved mixed portions [122]. Given their high lattice resistance, the glide of screw dislocations is thermally activated, resulting in a marked temperature and strain-rate dependence of the yield stress at low temperatures [123,6]. The reason behind this unconventional low-temperature plastic behavior is the core structure of the $1/2\langle 111\rangle$ screw dislocation, which has been debated at length in the literature, as already mentioned in the Introduction.

There is now a general consensus, reached in large part thanks to DFT calculations, that in pure BCC transition metals, the low-energy stable core configuration of the screw dislocation is symmetrical, or non-degenerate, as shown in Fig. 8a. This configuration, called the easy core, is centered on a triangle of first-neighbor $\langle 111\rangle$ atomic columns, where helicity is reversed compared to the bulk [33,60,69,82,85,86,88,124–127]. The concept of polarization was introduced to allow for a continuous description from a non-degenerate unpolarized core to a fully polarized degenerate core [128,129]. DFT calculations of the dependence of the easy core energy on polarization (Fig. 8d) confirm that in pure metals, the stable

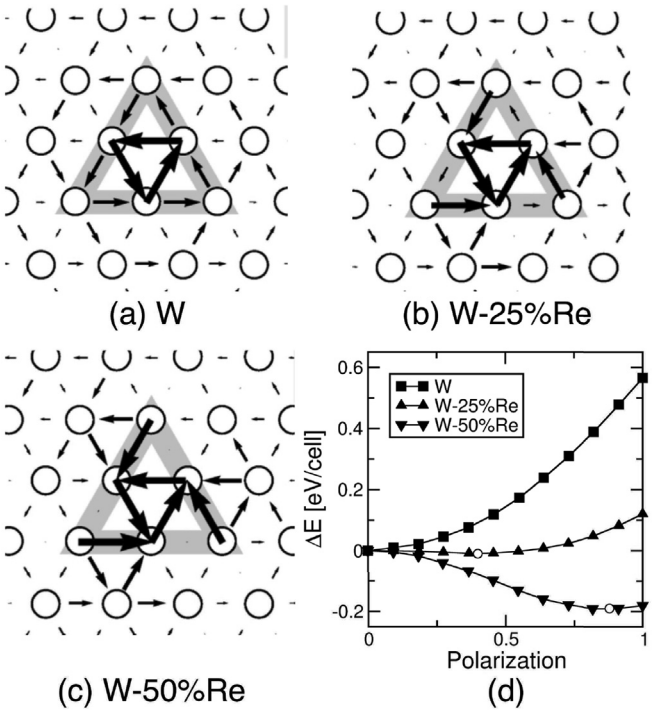

Fig. 8. Easy core structure of a 1/2⟨111⟩ screw dislocation in (a) pure W, (b) $W_{0.75}Re_{0.25}$ and (c) $W_{0.50}Re_{0.50}$ alloys predicted with DFT using a virtual crystal approximation. The core is visualized using differential displacement arrows between ⟨111⟩ columns. (d) Dependence of the dislocation core energy on polarization. Open circles refer to minima at finite polarization. Adapted with permission from Refs. [81,137].

easy core is fully unpolarized [130]. The non-degenerate nature of the easy core can also be anticipated from the shape of the ⟨111⟩ cross-section of the {110} γ-surface. According to the work of Duesbery and Vitek [23], a non-degenerate core is expected when $2\gamma(b/6)<\gamma(b/3)$, which is predicted by DFT calculations [29,81,124,131–134]. We note also that a generalization of the Peierls-Nabarro model for non planar cores was shown able to predict correctly the dislocation core of the screw dislocation in bcc Ta [135]. Finally, none of the GSF calculations in BCC metals found a metastable stacking fault, in agreement with the absence of dissociated cores in these metals.

No metastable dislocation core configuration has been evidenced so far in pure BCC transition metals: the hard core, centered on a triangle where the three ⟨111⟩ atomic columns are at the same altitude, and the split core located in the immediate vicinity of a ⟨111⟩ atomic column [136] are both unstable.

The properties of the stable easy core configuration have been thoroughly investigated using first principles. Notably, the screw dislocation induces a displacement field in the ⟨111⟩ direction very close to the Volterra elastic field. In addition, there is a short-range dilatation core field, which can be modeled with anisotropic elasticity using force dipoles [60]. Also, the dislocation core energy was shown to depend on the filling of the d-band, in relation to the position of the Fermi level with respect to the minimum of the pseudogap of the electronic density of states [82]. Finally, in the case of Fe, the local atomic magnetic moments were found weakly perturbed by the presence of the screw dislocation, with a small increase of about 0.2 μ_B/atom according to DFT-GGA calculations [86], in agreement with locally self-consistent multiple scattering calculations [138].

4.2. The Peierls barrier

The elementary glide process of the 1/2⟨111⟩ screw dislocation involves a thermally-activated transition between two stable easy core configurations along a {110} plane, with a corresponding Peierls barrier. As illustrated in Fig. 4, DFT calculations on straight infinite screw dislocations in Fe [85,131,139] and other BCC metals [82,86,88] (see Table 3) have shown that the Peierls barrier has a single maximum, with a marked group-dependence on the height of the energy barrier, the so-called Peierls energy: metals from group V have a lower scaled energy barrier than metals from group VI and Fe [82].

Few interatomic potentials predict the correct non-degenerate core structure and most of these predict an incorrect double-humped Peierls barrier [142,143]. The reason is that these potentials predict a metastable split core, through which the dislocation passes when changing Peierls valleys, as first observed with simple ⟨111⟩ rigid string models of BCC cohesion [25]. We note that as argued by Gröger and Vitek [27], accounting for the angular dependence of the covalent bonding in transition metals favors the correct non-degenerate core, as for instance with bond-order potentials (BOPs) [144–146].

4.3. The Peierls stress

The Peierls stress can be estimated from the maximum derivative of the Peierls barrier as a function of the dislocation core position, assuming that the stress-dependence of the Peierls barrier can be neglected [147,148]. For this, an accurate evaluation of the dislocation position in the {111} plane is crucial. However, the dislocation position can not be uniquely defined, as discussed in Sec. 2 and the resulting Peierls stress estimates differ by about 20% [82].

In order to determine the Peierls stress more accurately, a pure shear stress can be directly applied in increments until the screw dislocation starts to glide. However, one has to ensure that the dislocation is well relaxed between each stress increment since the resulting Peierls stress is very sensitive to the maximum force criterion used for the relaxations and may be overestimated up to a factor of about two. This method coupled to flexible boundary conditions has been used in BCC Mo and Ta [37,69], as shown in Fig. 9. It has also been used in W with periodic boundary conditions

Table 3
Peierls barriers (in meV/b) obtained with DFT in BCC transition metals from group V (V, Nb and Ta), group VI (Mo and W) and Fe. All the calculations used either the LDA or GGA Perdew-Burke-Ernzerhof [92] exchange-correlation functional, except Ref. [140] that used the GGA Perdew-Wang [141] exchange-correlation functional.

	V	Nb	Ta	Mo	W	Fe
VASP PAW GGA	25 [88]	30 [88]	38 [88], 109 [64]	61 [88]	94 [88]	35 [85], 60 [139]
VASP PAW LDA			91 [88]			
VASP US LDA			98 [88]			
PWSCF PAW GGA						40 [86]
PWSCF PAW LDA						22 [86]
PWSCF US GGA	26 [82]	35 [82]	37 [82]	51 [82]	82 [82], 86 [140] (PW)	35 [82]
DFT++ US LDA			60 [70]	80 [70]		

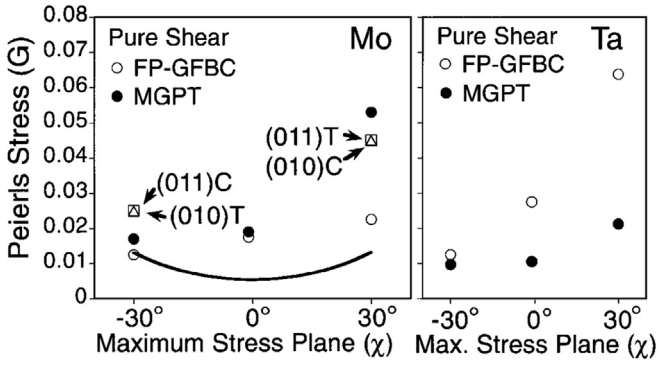

Fig. 9. Peierls stress variation with orientation of the maximum resolved shear stress plane (referred to by the χ angle relative to the {110} glide plane) in BCC Mo and Ta. The Peierls stress is in units of the shear modulus in the ⟨111⟩ direction (G). Reproduced with permission from Ref. [69].

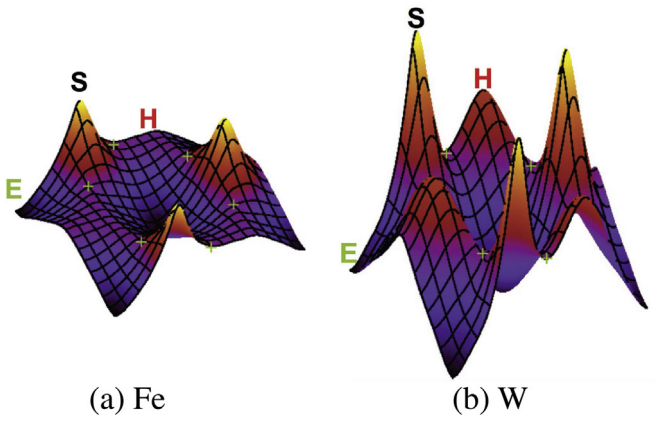

Fig. 10. 2D Peierls potentials for (a) Fe and (b) W. The colors scale with the energy between the minimum (dark) and the maximum energy (light). The symbols E, H and S denote the easy, hard and split cores respectively. Adapted with permission from Ref. [82]. (For interpretation of the references to colour in this figure legend, the reader is referred to the web version of this article.)

and an additional correction to account for the elastic interactions between dislocations [81]. Another method consists in determining the Peierls barrier under increasing applied stress until the barrier vanishes. Peierls barriers can be accurately obtained using periodic boundary conditions [78], provided that the energies are corrected for spurious elastic contributions of two origins: (1) under stress, the dislocations move in opposite directions and therefore their distance and elastic interaction energy vary along the path, and (2) the calculations use a fixed cell shape while the periodicity vectors should depend on the relative positions of the dislocations to maintain a constant applied stress.

Independently of the method used, all atomistic calculations, including DFT, evidence a discrepancy with experimental estimates of the Peierls stress. Several explanations have been proposed [149,150], including a role of zero-point vibrations [151,152]. Non-glide stresses, which have not been taken into account in the DFT calculations, probably also contribute to this discrepancy [26,149,152–154].

All calculations mentioned above were concerned with straight infinite dislocations and are thus limited to the 0 K limit. At finite temperatures, dislocation glide proceeds through the nucleation and propagation of kink pairs, which break translational invariance. So far, *ab initio* simulation cells have been too small to allow for a direct calculation of a finite-length dislocation with a kink or a kink pair [155]. However, kink-pair activation enthalpies can be predicted using input from DFT calculations, making use of an upscaling approach based on the line tension model [156,136].

4.4. Deviation from the Schmid law

As illustrated in Fig. 9, BCC metals are well-known for deviating from the Schmid law [23,123,157], according to which plastic flow starts when the shear stress parallel to the Burgers vector and resolved in the slip plane (the resolved shear stress) reaches a critical value. One manifestation is a tension-compression asymmetry in uniaxial loading tests [123], which is related to the so-called twinning/antitwinning (T/AT) asymmetry of shear of the BCC structure along the ⟨111⟩ direction parallel to {211} planes.

To account for the T/AT asymmetry on dislocation glide, Edagawa et al. [158,159] proposed in the 1990's to extend the definition of the Peierls potential to two dimensions, i.e. to the entire {111} plane, instead of only between easy core configurations as discussed above. The resulting 2D Peierls potentials have been investigated using DFT [82,85] and were found different from the landscapes commonly assumed based on empirical potential calculations. Fig. 10 shows examples in Fe and W. In particular, it was found that the split core has a high energy close or above that of the hard core. These calculations also evidence the atypical behavior of Fe, where the hard core appears to be a monkey saddle type of energy extremum, instead of a local maximum as in all other BCC metals.

In this landscape, the dislocation trajectory is not straight between equilibrium configurations [82,86,158]. The deviation has recently been directly linked to the magnitude of the T/AT asymmetry [78]. A projection of the applied shear stress on the current, deviated trajectory, instead of the average {110} glide plane, provides a modified Schmid law, which reproduces qualitatively low-temperature experimental data and quantitatively DFT calculations of the crystal orientation dependence the Peierls stress.

4.5. Alloying effects

So far, there has only been a limited number of DFT investigations of alloying effects in BCC metals. These studies include the interaction between straight screw dislocations and substitutional transition metal solutes in Mo, in connection with a solid-solution softening model of plasticity [126]. The model is based on DFT calculations of the solute-dislocation binding energy and of the stiffness for moving an atomic row in the dislocation core, which correlates with the magnitude of the Peierls stress. The atomic row model with *ab initio* parametrization of the interatomic interactions was used to study the trends of solid solution softening and hardening in Nb, Ta, Mo and W [160].

DFT calculations have also shown that alloying with substitutional elements can substantially modify the structure of a dislocation core. Using a virtual crystal approximation (VCA) based on virtual atoms interpolating between solvent and solute atoms, alloying by substitutional solutes (notably adding Co in Fe or in W, adding Re or group VIII transition metal elements, Fe, Ru and Os) was found to induce a transition from a symmetric to an asymmetric easy core configuration [81,137,140,161], as illustrated in Fig. 8a–c, where asymmetrical differential displacements develop around the dislocation core when the concentration of Re in W increases. Concomitantly, minima at finite polarization appear in the energy-polarization curves of Fig. 8d [137].

A few DFT calculations of the interaction energies between screw dislocations and interstitial solutes have been performed, in particular, H and He in Fe and W, using either flexible boundary conditions [162], periodic boundary conditions [163] or a QM/MM

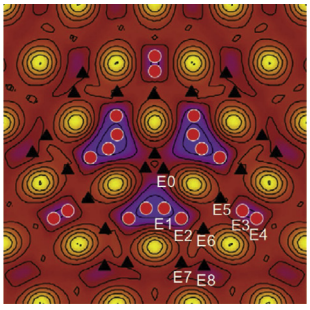

Fig. 11. Projection in the (111) plane of the hydrogen interstitial positions around the easy core configuration in Fe. The circles (respectively triangles) represent the interstitial positions with a binding energy to the screw dislocation larger (respectively smaller) than 100 meV. Colors and contours scale with electron density from dark (minimum) to bright (maximum). Adapted with permission from Ref. [162]. (For interpretation of the references to colour in this figure legend, the reader is referred to the web version of this article.)

approach [139]. Solute-dislocation interactions are systematically attractive when the solutes are within 4 Å from the core and strong attractions were found, with segregation energies up to 0.4 eV for H in Fe [162] (Fig. 11) and 0.5 eV for H in W [163] and He in Fe [139].

Solute-induced structural changes have also been evidenced with interstitial solutes. A recent DFT study has demonstrated that adding B, C, N or O solutes in Fe or adding C into W near a screw dislocation core destabilizes the easy core to the benefit of the hard core [164] (see Fig. 12). This unexpected reconstruction is associated with a strong solute-dislocation attraction and a segregation energy up to 0.8 eV per C atom in Fe. DFT calculations coupled to Eshelby's model were also employed to calculate C atom-dislocation interactions in Fe, but without explicitly including a dislocation core [165].

5. HCP metals

HCP metals are characterized by several potential slip systems,

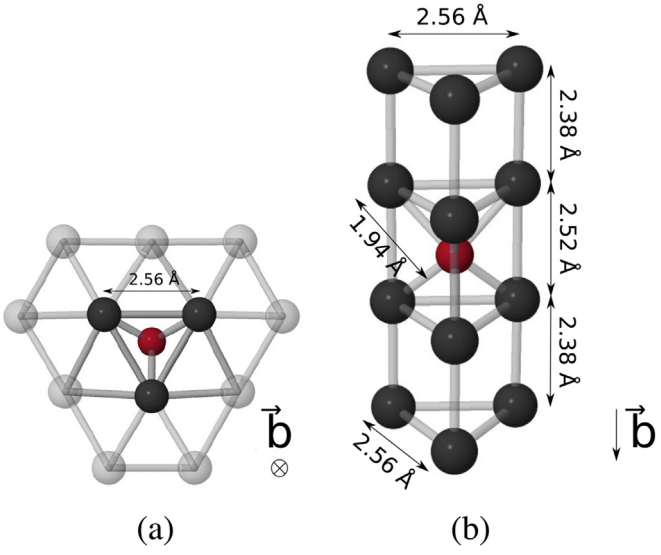

Fig. 12. Reconstruction into a hard core configuration of a 1/2⟨111⟩ screw dislocation in presence of C solute atoms. The C solute atoms (in red) are at the center of regular trigonal prisms formed by the Fe atoms in the three ⟨111⟩ atomic columns of the core (in dark gray). Adapted with permission from Ref. [164]. (For interpretation of the references to colour in this figure legend, the reader is referred to the web version of this article.)

with metal-dependent activities. The prevalent Burgers vector is systematically an ⟨*a*⟩ vector of the 1/3 ⟨$1\bar{2}10$⟩ type, but depending on the metal under consideration, ⟨*a*⟩ dislocations may glide most easily either in the basal (0001) or in a prismatic {$\bar{1}010$} plane (see Fig. 13a). Cross-slip of ⟨*a*⟩ dislocations in first-order pyramidal {$\bar{1}011$} planes is also observed. Since ⟨*a*⟩ dislocations cannot accommodate strain along the ⟨*c*⟩ axis of the HCP lattice, additional deformation modes are needed and may correspond to either twinning or ⟨*c*+*a*⟩ dislocations, *i.e.* dislocations with a 1/3 ⟨$2\bar{1}\bar{1}3$⟩ Burgers vector gliding either in the {$\bar{1}011$} first- or {$\bar{2}112$} second-order pyramidal plane shown in Fig. 13b. In the following, we consider first ⟨*a*⟩, then ⟨*c*+*a*⟩ dislocations. We will use Mg, Ti and Zr as representative HCP metals because they have been mainly considered by *ab initio* calculations and they offer an overview of the various plastic behaviors encountered in HCP crystals.

5.1. ⟨*a*⟩ dislocations

Like FCC dislocations, ⟨*a*⟩ dislocations in HCP metals dissociate into partial dislocations separated by a stacking fault. Legrand [166] showed that the choice between a primary basal or prismatic slip system can be rationalized based on the ratio between stacking fault energies in these planes, which are reviewed here.

5.1.1. Stacking faults

Various stable stacking faults responsible for dislocation dissociation are seen on the γ-surfaces of Fig. 15.

Basal plane. In all HCP metals, the γ-surface between basal planes (Fig. 15a) contains a single minimum at finite shear, which transforms the original …*BABABA*… stacking into …*BABCAC*…, with two planes with FCC environment. This intrinsic stacking fault, called I_2, is the opposite of that seen in FCC metals and leads to a similar dissociation, with two non-collinear partial dislocations satisfying:

$$\frac{1}{3}\left[1\bar{2}10\right] \rightarrow \frac{1}{3}\left[1\bar{1}00\right] + \frac{1}{3}\left[0\bar{1}10\right]. \quad (4)$$

As seen in Table 4, the I_2 stacking fault energy is low in Mg and high in Ti and Zr. Since the separation between first- and second-nearest neighbors is not modified by the basal fault [186], the higher fault energy in Ti and Zr is a consequence of the directional bonding induced by the valence *d* electrons in these transition metals.

Prismatic plane. As illustrated in Fig. 14, prismatic planes are corrugated (or rumpled [187]) and define closely- and loosely-spaced planes. Calculations in Ti [55,176,177] and Mg [188,189]

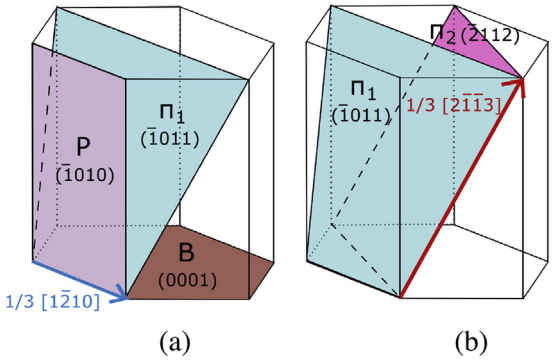

Fig. 13. Hexagonal close-packed structure showing the different potential glide planes of (a) ⟨*a*⟩ and (b) ⟨*c*+*a*⟩ dislocations.

Table 4
Summary of *ab initio* results in HCP metals: lattice parameters a and c; stacking fault energies γ_b, γ_p and γ_π respectively in the (0001) basal, the $\{\bar{1}010\}$ P_L prismatic and the $\{\bar{1}011\}$ π_{1D} first-order pyramidal planes relevant for $\langle a\rangle$ dislocations; elastic constants C_{ij}; and ratio $R = C_{66}\gamma_b/C_{44}\gamma_p$ to predict the primary glide system (prismatic for $R > 1$ and basal for $R < 1$) [166].

Method[a]	a (Å)	c/a	Faults (mJ m^{-2})			Elastic constants (GPa)					R[b]
			γ_b	γ_p	γ_π	C_{11}	C_{33}	C_{44}	C_{66}	C_{13}	
Mg: Expt [167,168].	3.21	1.623				59	61	16	17	21	B
VASP PW PAW [169]	3.20	1.620	34	354[c]							
VASP PW US 2e [89,90]	3.19	1.624	34	218[c]		60	61	18	19	20	0.16
VASP PW PAW 2e [90,91]	3.19	1.624	34	216		61	62	19	20	21	0.17
VASP PBE PAW [170]	3.189	1.626	37	231[c]							
VASP PBE PAW [171,172]			35	169[c]							
Ti: Expt [167,173].	2.951	1.585				176	190	51	45	68	P
VASP PW US 10e [174,175]	2.940	1.589	291	174				43	45		1.8
VASP PW US 4e [176]	2.934	1.582	336	206							1.7
VASP PW PAW 4e [177,178]	2.920	1.581	292	220		169	189	37	36	84	1.3
VASP PW US 10e [178]	2.949	1.580		264		164	190	42	37	75	
VASP PBE PAW 4e [55,179]	2.94	1.583	306	203	205						
PWSCF PBE US 12e [77,180]	2.936	1.583	297	256	227	169	192	42	40	77	1.1
VASP PBE PAW 4e [181]	2.924	1.587	309	213	205	186	191	47	49	84	1.5
Zr: Expt [167,173].	3.232	1.603				155	172	36	44	65	P
VASP PW US 10e [34,182,183]	3.23	1.604	200	145		142	164	29	39	64	1.8
VASP PBE PAW [184]	3.23	1.601	227	197		156	166	26	47	62	2.1
VASP PW US 4e [176]	3.209	1.602	213	166							1.4
PWSCF PBE US 12e [84,77]	3.230	1.601	213	211	163	140	168	26	35	65	1.4

[a] PW: GGA exchange-correlation functional parameterized by Perdew and Wang [141]; PBE: Perdew, Burke, and Ernzerhof GGA functional [92]; US: ultra-soft pseudo-potential [185]; PAW: projected augmented wave method; *ne*: number of electrons in valence state.
[b] For experimental data, the principal glide plane, either basal or prismatic, is indicated as B or P.
[c] Unstable.

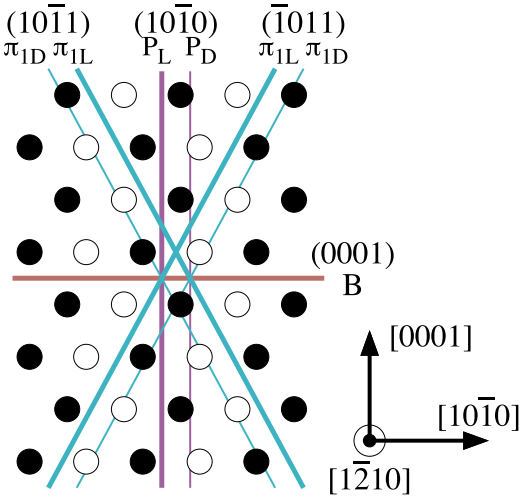

Fig. 14. Projection perpendicular to [1$\bar{2}$10] showing the different potential glide planes for a $\langle a\rangle$ screw dislocation. Atoms are sketched by circles with a color depending on their (1$\bar{2}$10) plane. Loose and dense planes are drawn respectively with a thin and a thick line, both for prismatic and first-order pyramidal planes. (For interpretation of the references to colour in this figure legend, the reader is referred to the web version of this article.)

have shown that it is easier to shear along a $\langle 1\bar{2}10\rangle$ direction between two loose planes (P_L plane in Fig. 14), which is the only case considered below, rather than between close planes (P_D in Fig. 14).

As shown in Fig. 15b and found in both Ti [52,55,77,174–180] and Zr [34,84,174,176,182–184], the prismatic γ-surface shows a valley along [1$\bar{2}$10], with a minimum at half a periodicity vector, indicating a stable stacking fault in this direction. $\langle a\rangle$ dislocations are therefore expected to dissociate in Ti and Zr according to:

$$\frac{1}{3}\left[1\bar{2}10\right] \rightarrow \frac{1}{6}\left[1\bar{2}10\right] + \frac{1}{6}\left[1\bar{2}10\right]. \quad (5)$$

The prismatic stacking fault energy in Ti and Zr is usually found lower than the basal stacking fault (Table 4). However, Udagawa et al. [184] and Benoit et al. [52] have shown that this energy strongly depends on the number of atomic planes included in the simulation cell when a slab geometry is used instead of full periodic boundary conditions, as mentioned in Sec. 2. Also, we should note that the stacking fault obtained *ab initio* in Ti is significantly lower than deduced from experiments. De Crecy et al. [190] observed with high resolution TEM an edge dislocation dissociated in a prismatic plane in Ti with a dissociation width $d_p = 12$ Å. The original fault energy deduced from isotropic elasticity with partial Burgers vectors of $a/3$ and $2a/3$ was $\gamma_p = 150$ mJ m^{-2}. Corrections using anisotropic elasticity [191,173] and $a/2$ partial vectors yield $\gamma_p = (C_{11}^2 - C_{12}^2)a^2/(8\pi C_{11} d_p) = 159$ mJ m^{-2}, a value which remains about 25% lower than from first-principles. The origin of this discrepancy remains unknown to this date.

The 1/6[1$\bar{2}$10] fault vector corresponds to a maximum in Mg [89–91,192–196] and the energy of this unstable fault is much higher than the basal stacking fault (Table 4). Using PAW, Yasi et al. [90,91] found a shallow minimum at 1/6[1$\bar{2}$10] + 0.065[0001], but the corresponding energy (216 mJ m^{-2}) is very close to the unstable stacking fault (218 mJ m^{-2}). In contrast with Ti and Zr, the γ-surface of Mg is close to that obtained with central-force potentials, or even hard sphere models, which invariably predict an energy maximum at 1/6 [1$\bar{2}$10] and a stable stacking fault at 1/6[1$\bar{2}$10] + α[0001] with $\alpha \neq 0$ [186].

Pyramidal planes. First-order pyramidal planes are also corrugated. Most *ab initio* studies have considered GSFE between widely spaced planes (π_{1L} in Fig. 14), where no minimum is found near the $\langle a\rangle$ direction. This γ-surface is however more relevant for $\langle c+a\rangle$ dislocations and will be discussed in Sec. 5.2.

Ab initio calculations in Zr and Ti [55,77,197] showed that it is in fact easier to shear the HCP crystal along the $\langle a\rangle$ direction between closely spaced planes (π_{1D} in Fig. 14). An example is shown for Ti in Fig. 15c. There is a minimum at 1/6 [1$\bar{2}$10] + α[10$\bar{1}$2] with $\alpha \neq 0$, but the stable stacking fault fully develops only after full atomic relaxation [77] or NEB calculations [55]. Analysis of the atomic

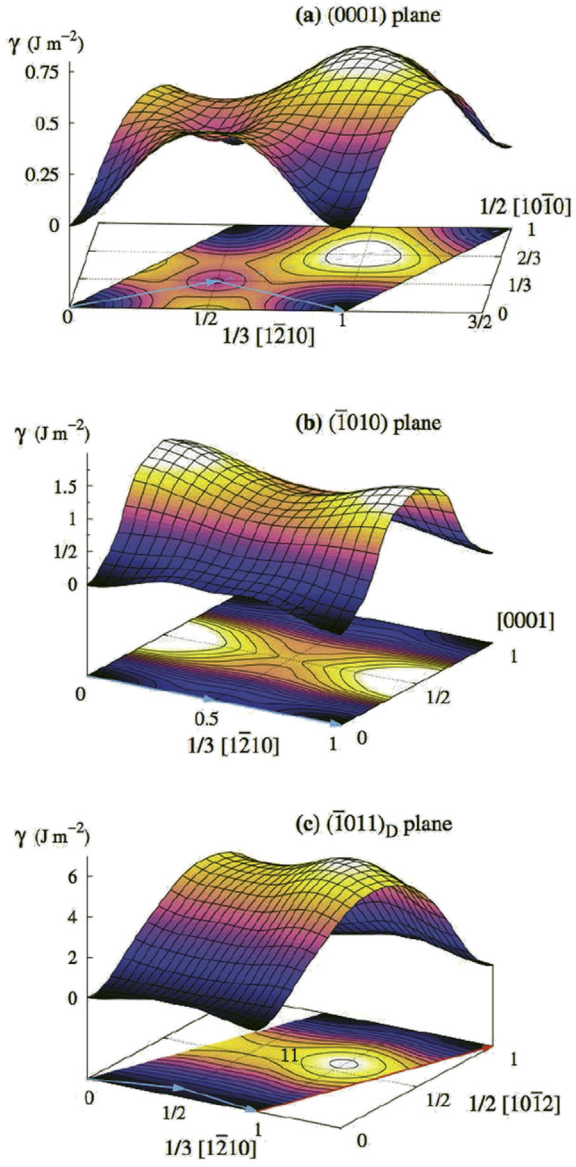

Fig. 15. GSFE surface in Ti for (a) the basal, (b) the prismatic, and (c) the first-order pyramidal planes. The fault plane is the loose P_L plane in (b) and the dense π_{1D} plane in (c). Data were obtained with PWSCF in the GGA approximation. The blue and red arrows indicate the possible dissociation of respectively 1/3 [1$\bar{2}$10] and 1/3 [2$\bar{1}\bar{1}$3] Burgers vectors. (For interpretation of the references to colour in this figure legend, the reader is referred to the web version of this article.)

structure shows that this pyramidal stacking fault is an elementary two-layer pyramidal twin [77,197]. The HCP structure can be described in the pyramidal direction as a stacking of corrugated planes …*ABCDEFG*… without repeatable sequence. The pyramidal stacking fault then corresponds to the introduction of two mirror planes, leading to …*ABCDCBCDE*…. The theoretical fault vector is therefore the Burgers vector of the two-layer disconnection for the {$\bar{1}$011} twinning system [198], and an ⟨*a*⟩ dislocation is expected to dissociate in a first-order pyramidal plane according to:

$$\frac{1}{3}\left[1\bar{2}10\right] \rightarrow \left(\frac{1}{6}\left[1\bar{2}10\right] + \frac{4c^2 - 9a^2}{2(4c^2 + 3a^2)}\left[10\bar{1}2\right]\right) + \left(\frac{1}{6}\left[1\bar{2}10\right] - \frac{4c^2 - 9a^2}{2(4c^2 + 3a^2)}\left[10\bar{1}2\right]\right). \quad (6)$$

Stable pyramidal stacking faults have been obtained in both Ti and Zr [55,77,181,197], with an energy usually slightly lower than the prismatic stacking fault (Table 4). Because this pyramidal stacking fault is strongly related to {$\bar{1}$011} twinning, which is active in most HCP metals, we expect this stacking fault is stable in HCP crystals other than Ti and Zr.

Primary glide system. The criterion proposed by Legrand [166] predicts a dissociation in a basal plane, and therefore a primary basal slip system, if the ratio $R = C_{66}\gamma_b/C_{44}\gamma_p$ is less than 1. Otherwise, the dissociation and primary slip system are prismatic. Using this criterion with *ab initio* stacking fault energies and elastic constants, we recover that the primary slip system is basal in Mg and prismatic in Ti and Zr, in agreement with experiments. This criterion however does not consider dissociation in the first-order pyramidal plane.

5.1.2. Titanium and zirconium

Pure metals. For the ⟨*a*⟩ screw dislocation, *ab initio* calculations have identified three core structures common to Ti [175,177,180,199–201] and Zr [34,35,77,84,175,180,197]. As expected from the GSFEs, the screw dislocation dissociates in a prismatic plane (Fig. 16c), with two *a*/2 partial dislocations (Eq. (5)). A core dissociated in a first-order pyramidal plane has also been found (Fig. 16a) in agreement with Eq. (6). In addition, an unexpected non-planar configuration with the dislocation spread in both prismatic and pyramidal planes has also been identified (Fig. 16b). Note that dissociation in the basal plane (Eq. (4)) is unstable in both Ti [200] and Zr [84].

All three configurations (prismatic, pyramidal and non-planar) are stable in Ti and Zr, but with different relative stabilities [180]. The minimum energy configuration in Zr is dissociated in the prismatic plane (Fig. 16c) and can easily glide in this plane with a low Peierls barrier (< 0.3 meV Å^{-1}) [84]. The estimated Peierls stress is lower than 21 MPa, in agreement with single-crystal experiments [202–205]. This prismatic configuration can also glide in pyramidal and basal planes, but with a high Peierls barrier, which in both cases passes through the non-planar metastable core of Fig. 16b [77,197]. Glide of ⟨*a*⟩ dislocations is therefore confined at low temperatures in Zr to prismatic planes, while cross-slip in pyramidal and basal planes may only be activated at high temperatures.

In Ti, the minimum energy configuration of the screw dislocation is the pyramidal core of Fig. 16a with a high Peierls barrier, ~11.4 meV Å^{-1}. Experimentally, dislocation glide in Ti is jerky but mainly along prismatic planes [206,207]. A locking-unlocking mechanism was therefore proposed [180], whereby the stable but sessile pyramidal core cross-slips in a prismatic plane, where it is only metastable (the energy difference between prismatic and pyramidal cores is ~5.7 meV Å^{-1}), but can glide over large distances with a low Peierls barrier (<0.4 meV Å^{-1}) before returning to the sessile pyramidal core.

Alloying effects. The plastic behaviors of Ti and Zr alloys is strongly influenced by the presence of interstitial impurities, like O, C, N, and S [208–210]. These impurities all lie in the octahedral interstitial sites of the HCP lattice and lead to a marked hardening, which cannot be associated with a simple elastic interaction between dislocations and impurities [211], but involves a modification of the dislocation core structure [201].

Except a few early *ab initio* calculations in small sized systems, which considered H [34,174] and S [35], only O interstitials have been studied so far [201,212]. Calculations in both Ti and Zr evidenced significant interactions when the O atom lies in the ⟨*a*⟩ screw dislocation habit plane. A strong repulsion is obtained for O positions, which correspond to octahedral sites of the HCP lattice

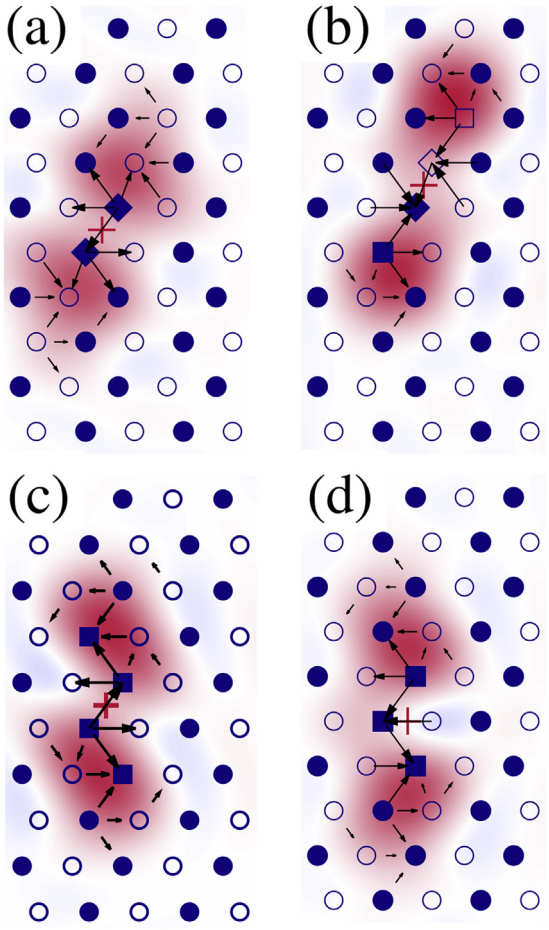

Fig. 16. Core structures of a screw $\langle a \rangle$ dislocation in Ti. Configurations (a), (b) and (c) are stable, (d) is unstable. Atoms are sketched by symbols with a color depending on their $(1\bar{2}10)$ plane in the original perfect crystal. Different symbols are used for atoms depending on their neighborhood in the dislocated crystal, *i.e.* close to a perfect crystal (circles), in a $(\bar{1}011)$ pyramidal stacking fault (diamonds), or a $(\bar{1}010)$ prismatic stacking fault (squares). Arrows between atomic columns show differential displacements in the $[1\bar{2}10]$ direction. The contour map shows the dislocation density according to the Nye tensor and the red crosses indicate the position of the dislocation center. (For interpretation of the references to colour in this figure legend, the reader is referred to the web version of this article.)

that are destroyed when the prismatic dislocation dissociates (green squares in Fig. 17a and b) [178,179,201]. Because of this strong repulsion, the dislocation partially cross-slips to an adjacent prismatic plane (Fig. 17a and b), favoring cross-slip as observed experimentally [211,201].

The stacking fault ribbon created by the screw dislocation also creates new insertion sites for the O atoms (green diamond in Fig. 17a and c) [178,179,201]. They also result in a repulsive interaction, but not strong enough to induce cross-slip (Fig. 17a and c) [201,212]. The screw dislocation may therefore minimize its repulsion with O atoms by shuffling between old and new octahedral sites [201].

5.1.3. Magnesium

Pure metals. In agreement with the Legrand criterion, *ab initio* calculations [75,89,91,213] have shown that $\langle a \rangle$ dislocations in Mg are most stable when dissociated in a basal plane. Both edge [89] and screw [75,89,91,213] $\langle a \rangle$ basal dislocations have been modeled. As expected from the GFSEs (Eq. (4)), the dislocations dissociate in two Shockley partials separated by an I_2 stacking fault

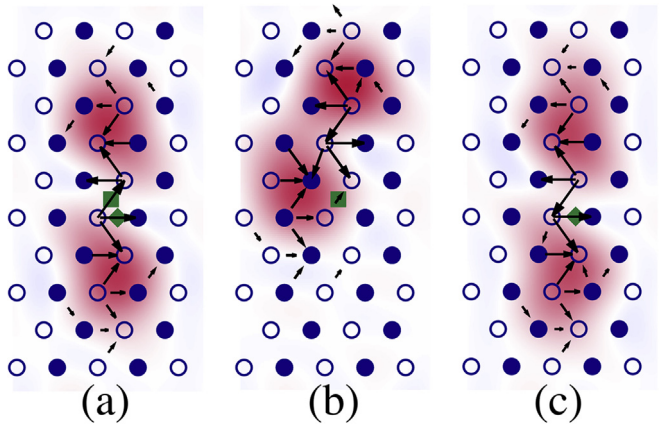

Fig. 17. Core structure of a screw $\langle a \rangle$ dislocation in Zr in presence of an O impurity. The initial configuration of the dislocation, before introduction of the O atom, is shown in (a). The relaxed structures are shown in (b) and (c) for an O atom lying respectively in an octahedral site destroyed (green square) and created (green diamond) by the prismatic stacking fault. (For interpretation of the references to colour in this figure legend, the reader is referred to the web version of this article.)

(Fig. 18). The splitting distances, deduced from the maxima of the Nye tensor, are 5.2 a and 2.0 a for the edge and the screw dislocations, respectively (a ~ 3.2 Å is the lattice parameter) [89]. Moreover, two configurations of the screw dislocation separated by half a Peierls valley [213] were stabilized. The corresponding energy difference (1 meV b^{-1}) is the Peierls barrier, thus showing that screw dislocations can easily glide in basal planes in Mg, as confirmed by NEB calculations [75].

Using a pseudopotential approximation, the edge dislocation lying in a prismatic plane has a compact core, whereas the screw

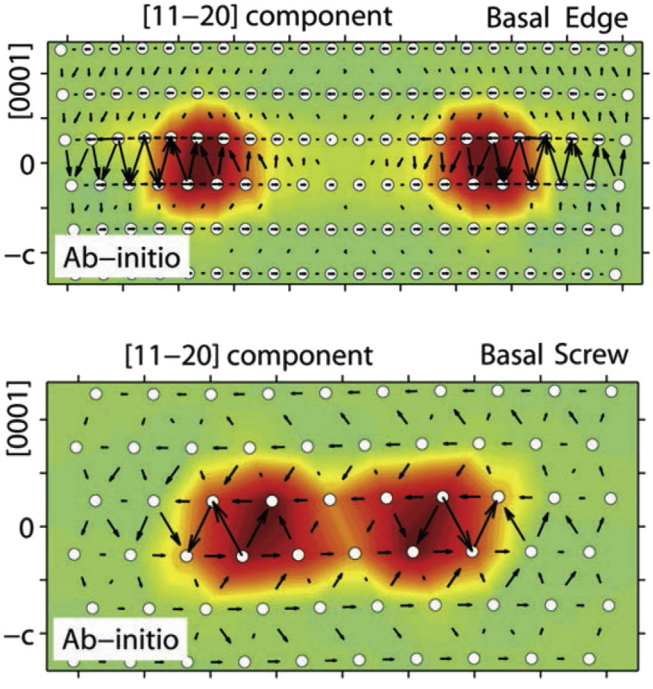

Fig. 18. Core structure of an edge and a screw $\langle a \rangle$ dislocation lying in a basal plane in Mg. The color map indicates the dislocation densities corresponding to the edge and the screw components of the Nye tensor and the arrows show the corresponding differential displacements. Adapted with permission from Ref. [89]. (For interpretation of the references to colour in this figure legend, the reader is referred to the web version of this article.)

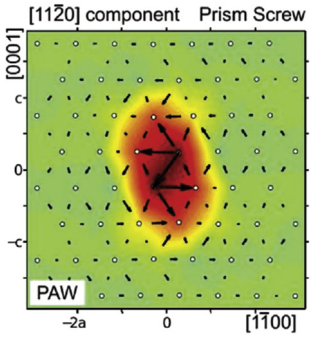

Fig. 19. Core structure of a screw ⟨*a*⟩ dislocation in a prismatic plane in Mg. The color map indicates the dislocation densities corresponding to the screw components of the Nye tensor and the arrows show the corresponding differential displacements. Reproduced with permission from Ref. [90]. (For interpretation of the references to colour in this figure legend, the reader is referred to the web version of this article.)

dislocation is unstable [89] and spontaneously redissociates in the basal plane. However, using the more accurate PAW formalism, a prismatic configuration of the screw dislocation may be stabilized [75,91,213], in agreement with GSFE calculations, which show a shallow minimum in the prismatic γ-surface only with PAW, as mentioned above. This prismatic screw configuration remains rather compact (Fig. 19) and can be stabilized in two different positions separated by half a Peierls valley [213] like the basal core. The corresponding energy difference, $\lesssim$1.5 meV b^{-1}, is small, indicating that this prismatic screw dislocation is glissile. On the other hand, this core is metastable and marginally stable compared to the basal configuration because it has an excess energy of 61 ± 2 meV b^{-1} and is separated from the basal core by a negligible energy barrier [213]. A metastable glissile prismatic core is however in agreement with the locking-unlocking cross-slip mechanism proposed to explain prismatic glide at low temperatures observed experimentally in Mg [214].

NEB calculations for prismatic glide of basal dislocations have also been performed [75], showing that the dislocation first constricts to adopt a compact prismatic core, then moves in the prismatic plane and finally dissociates back in the neighboring basal plane. The energy barrier is then controlled by the constriction and corresponds to the energy difference between basal and prismatic configurations. Tsuru and Chrzan [75] further showed that this energy variation can be traced back to the occupation of the electronic *p*-states of Mg atoms in the dislocation core.

Alloying effects. Direct *ab initio* calculations of the interaction between a solute atom and an edge [215] or a screw dislocation [75,91,188,215] have been performed. Al and Zn solutes do not perturb the basal dissociation [215,75], whereas Y, Ca, Ti and Zr solutes destabilize the basal screw configuration and promote the compact prismatic core [75], due to an hybridization of the electronic *d*-states of the solutes with the *p*-states of Mg core atoms. The compact core can be further stabilized by segregation of Ca, K, Na or Sc [91,188]. The prismatic configuration is stable with K and Na whatever their substitution site, while Ca and Sc promote the basal core for some substitution sites. With Y and Zr, all sites in the dislocation core destabilize the prismatic configuration, despite an attractive interaction with the prismatic stacking fault [188].

These *ab initio* calculations have been used to validate mesoscopic models describing the interaction as a sum of size misfits and an interaction with the stacking fault [91,188,215] so as to predict solid-solution hardening for basal glide [215] or activation of prismatic cross-slip by solute addition [91,188].

5.2. ⟨*c*+*a*⟩ dislocations

Dislocations with a ⟨*c*+*a*⟩ Burgers vector can glide either in the π_1 first-order or π_2 second-order pyramidal planes (Fig. 13b). Glide is usually observed in π_1 planes in Zr [216] and Ti [217,218], although glide in π_2 planes has been reported in Ti [219]. By way of contrast, in Mg, both planes are observed [220–223].

5.2.1. Stacking faults

First-order pyramidal plane. As shown in Fig. 20, while the γ-surface between loosely-spaced π_{1L} planes does not show any minimum near the ⟨*a*⟩ direction, calculations in both Mg [224], Ti [181,225] and Zr [197,212] found a minimum near the ⟨*c*+*a*⟩ direction, at $\alpha[10\bar{1}2]$ with α close to 1/4 after full relaxation (Table 5).

Similarly to the pyramidal π_{1D} fault responsible for the dissociation of ⟨*a*⟩ dislocations (see Sec. 5.1), this π_{1L} pyramidal fault is related to $\{\bar{1}011\}$ $\langle 10\bar{1}2\rangle$ twinning. The fault changes the …*ABC-DEF*… stacking of corrugated pyramidal planes into …*ABC*|*BCD*…, with two mirror planes *C* and *B*. The atomic structure therefore corresponds to a $\{\bar{1}011\}$ incipient twin with a height of a single atomic layer. The theoretical fault vector is the Burgers vector of the disconnection of unit height, $3a^2/(3a^2+4c^2)$ $\langle 10\bar{1}2\rangle$, leading to 9/41 $\langle 10\bar{1}2\rangle$ for an ideal *c*/*a* ratio, which is close to the α~1/4 found above numerically, as well as with high resolution TEM in Mg [227].

Since the energy of this stacking fault is low (Table 5) and the

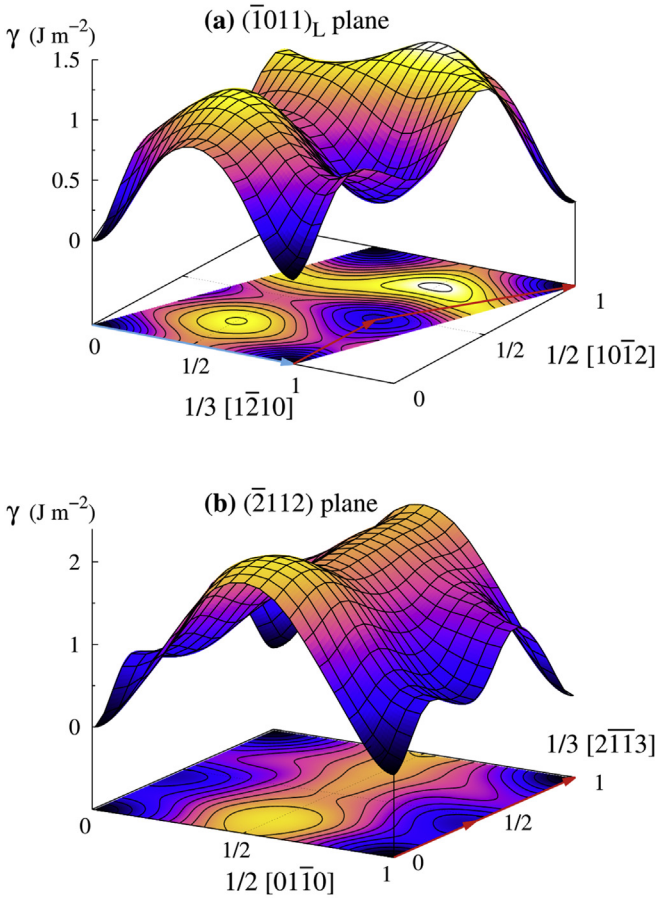

Fig. 20. GSFE surface in Ti for the (a) first- and (b) second-order pyramidal planes. The fault plane is the loose π_{1L} plane in (a). Data were obtained with PWSCF in the GGA approximation. The red arrows indicate the possible dissociation of the 1/3 [2$\bar{1}\bar{1}$3] Burgers vector. (For interpretation of the references to colour in this figure legend, the reader is referred to the web version of this article.)

Table 5
Stacking faults predicted by *ab initio* in the $(\bar{1}011)$ π_{1L} first-order and $(\bar{2}112)$ π_2 second-order pyramidal planes.

Method[a]	π_{1L} fault		π_2 fault	
	Vector	γ (mJ m)−2	Vector	γ (mJ m)−2
Mg:VASP PW PAW [169]			1/6 $[2\bar{1}\bar{1}3]$	399[b]
VASP PW US 2e [224]	0.25 $[10\bar{1}2]$	180[b]	0.11 $[2\bar{1}\bar{1}3]$	236[b]
VASP PBE PAW [170]			0.14 $[2\bar{1}\bar{1}3]$	318[b]
VASP PBE PAW [171,172]			1/6 $[2\bar{1}\bar{1}3]$	182 (236[b])
Ti:VASP PBE PAW 4e [55,179]	undefined	148 (430[b])		
VASP PBE PAW 4e [181]	0.215 $[10\bar{1}2]$	134 (243[b])	0.19 $[2\bar{1}\bar{1}3]$	297 (416[b])
PWSCF PBE US 12e [225]	0.212 $[10\bar{1}2]$	168 (242[b])	0.15 $[2\bar{1}\bar{1}3]$	375 (472[b])
Zr:VASP PW US 10e [174]	0.25 $[10\bar{1}2]$	240[b]	1/6 $[2\bar{1}\bar{1}3]$	400[b]
PWSCF PBE US 12e [197,212,226]	0.212 $[10\bar{1}2]$	127 (215[b])		

[a] *cf.* Table 4 for abbreviations.
[b] Atomic relaxations only in the direction perpendicular to the fault plane.

norm of the $\langle c+a\rangle$ Burgers vector is large, $\langle c+a\rangle$ dislocations are expected to dissociate in first-order pyramidal planes according to the following non-collinear reaction:

$$\frac{1}{3}\left[2\bar{1}\bar{1}3\right] \rightarrow \alpha\left[10\bar{1}2\right] + \left(\frac{1}{3}\left[2\bar{1}\bar{1}3\right] - \alpha\left[10\bar{1}2\right]\right).$$

Second-order pyramidal plane. γ-surfaces for π_2 planes, that are not corrugated, exhibit a valley along the $\langle c+a\rangle$ direction (Fig. 20b) with a minimum at $\alpha\,[2\bar{1}\bar{1}3]$ with α~1/6 after full relaxation (Table 5). This fault vector is close to one half the $\langle c+a\rangle$ Burgers vector [228,172] and corresponds to a local inversion of the … *ABAB*… basal stacking into …*BABA*… with a perfect alignment of the *A* and *B* basal planes along the pyramidal fault. This stable fault has been found in Mg [172,189,228,229], Ti [181] and Zr [228,174]. $\langle c+a\rangle$ dislocations are therefore expected to dissociate in the π_2 plane according to:

$$1/3\left[2\bar{1}\bar{1}3\right] \rightarrow 1/6\left[2\bar{1}\bar{1}3\right] + 1/6\left[2\bar{1}\bar{1}3\right],$$

in agreement with TEM observations in Mg-Y alloys [220].

Basal fault. Although the $\langle c+a\rangle$ vector does not belong to the basal plane, a correlation between the glide of $\langle c+a\rangle$ dislocations and the I_1 basal stacking fault has been established. Dislocation loops lying in a basal plane have been seen by TEM when glide of $\langle c+a\rangle$ is activated [222,230,231]. These basal loops are either faulted or dissociated in their habit plane, with a basal I_1 stacking fault involved in both cases. The vector of this basal fault is $1/6\left\langle 20\bar{2}3\right\rangle$ and a non conservative dissociation of $\langle c+a\rangle$ dislocations in the basal planes has been proposed with the following reaction

$$1/3\left[2\bar{1}\bar{1}3\right] \rightarrow 1/6\left[20\bar{1}3\right] + 1/6\left[02\bar{2}3\right],$$

as observed with TEM in Mg-Y alloys [232,220]. Although the precise mechanism for such a non conservative dissociation is not known [233], *ab initio* calculations have shown that the solute effect on the activity of $\langle c+a\rangle$ dislocations in Mg can be rationalized through a dependence of the basal I_1 stacking fault on solute content [232].

5.2.2. Dislocation core structures

Edge and screw $\langle c+a\rangle$ dislocations have been modeled with DFT, but only in Mg [178,235]. Ghazisaeidi et al. [178] used a cluster approach with fixed boundary conditions for the edge dislocation and flexible boundary conditions for the screw dislocation. Starting initially with either a dissociated or a compact core, the edge $\langle c+a\rangle$ dislocation lying in the π_2 plane dissociates in its habit plane in two collinear $1/2\langle c+a\rangle$ partials, without orthogonal component, as suggested by the pyramidal π_2 fault discussed above (Fig. 21). The resulting dissociation distance is ~18 Å. For the screw dislocation, a core initially dissociated in the π_2 plane remains dissociated with a dissociation distance of ~16 Å and $1/2\langle c+a\rangle$ partial Burgers vectors. On the other hand, starting from a compact core, the screw dislocation remains compact, but with an energy $\approx$0.32 eV b^{-1} higher than the dissociated core. Using periodic boundary conditions, Itakura et al. [235] obtained the same configuration dissociated in a π_2 plane for the screw dislocation, but showed that non planar cores also exist with stacking faults lying both in the π_1 and the π_2 planes. Such a non planar core is obtained for instance when the

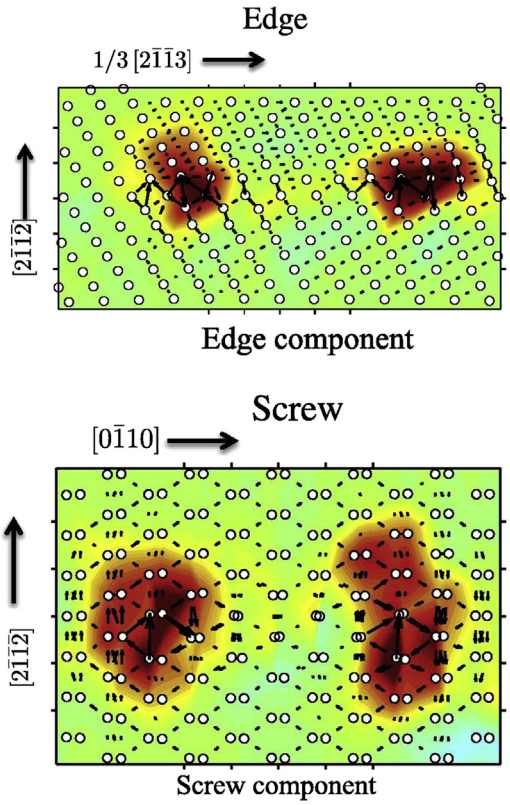

Fig. 21. Core structure of edge and screw $\langle c+a\rangle$ dislocations computed with DFT in Mg. The color map indicates the dislocation densities corresponding to the edge and screw components of the Nye tensor and the arrows show the corresponding differential displacements. Adapted with permission from Ref. [234]. (For interpretation of the references to colour in this figure legend, the reader is referred to the web version of this article.)

screw dislocation is initially dissociated in a π_1 plane. The screw dislocation can spontaneously transform from one core to the other under an applied strain, thanks to a shuffle of the atoms in the pyramidal stacking faults, an indication of the ease of cross-slip between both pyramidal planes.

Atomistic simulations relying on empirical potentials point to the existence of other possible core structures for the $\langle c+a\rangle$ dislocations, for instance locking configurations of the edge dislocation, corresponding either to a non-conservative dissociation in relation with the basal I_1 stacking fault or to the reaction $\langle c+a\rangle \rightarrow \langle c\rangle + \langle a\rangle$ [236]. However, these configurations and reactions have yet to be confirmed with *ab initio*.

6. Semiconductors

As mentioned in Introduction, the first *ab initio* calculations of dislocation cores were performed around the 1990's in semiconductors (see for instance Refs. [32,237]). One reason is that for a semiconductor like Si, an accurate description of the electronic structure can be obtained using a small number of k-points and a modest wave function basis. Also, core and Peierls energies in semiconductors are typically one order of magnitude larger than in metals, thus decreasing the relative errors. A third reason was the need to determine the influence of dislocation cores on electronic properties for application in electronics and optoelectronics [238].

6.1. Crystallography of semiconductors

Although a rather broad range of materials can be categorized as semiconductors, we will focus here on crystalline inorganic solids, namely on group IV elemental and group III-V and II-VI compound systems, which crystallize in the cubic diamond, zinc-blende or hexagonal wurtzite structures. We also include carbon diamond, which is not a semiconductor but has similar dislocation properties.

The cubic diamond and zinc-blende structures are formed of two interpenetrated FCC lattices, separated by $\sqrt{3}/4[111]$. For this reason, semiconductor and FCC dislocations share common features, for example, {111} glide planes. There is however one crucial difference illustrated in Fig. 22. In semiconductors, there are two inequivalent families of {111} planes, one forming narrowly spaced atomic layers, called the glide set, and the other, widely spaced atomic layers, called the shuffle set. The same type of relation exists between wurtzite and HCP lattices.

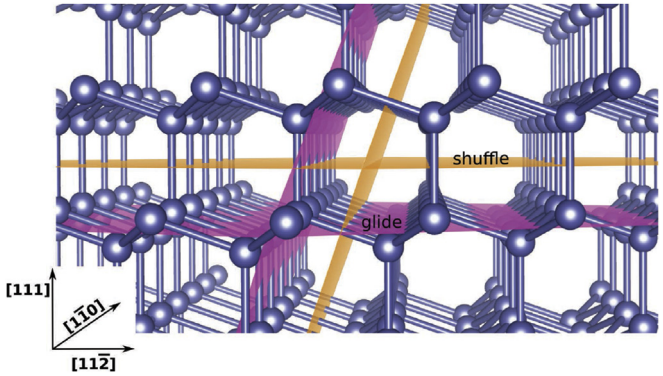

Fig. 22. Ball-and-stick representation of the cubic diamond structure with an orientation adapted for dislocation modeling, showing {111} glide planes in pink and shuffle planes in orange. (For interpretation of the references to colour in this figure legend, the reader is referred to the web version of this article.)

6.2. Core structure and stability

Semiconductors are characterized by a very large number of potential stable dislocation cores, depending on the dislocation character, glide plane and whether the system is a compound or a pure element. Most reported first-principles calculations use plane wave DFT with periodic boundary conditions and compare the relaxed energies of various potential candidates for a given simulation cell size. As mentioned in Sec. 2, this assumes that boundary condition effects are limited to the long-range elastic interactions between the dislocations and their periodic images and thus cancel in the energy differences if the candidates have the same character and Burgers vector. All reported calculations were performed at 0 K, except one investigation [239], which suggested that finite temperature corrections to free energy differences may amount to a few tens of meV Å^{-1}.

6.2.1. Shockley partial dislocations in the glide set

Cubic semiconductors. In the ductile regime above the brittle-to-ductile transition (BDT) characteristic of semiconductors [240], plastic deformation in cubic semiconductors involves the slip of 1/2 $\langle 110\rangle$ screw and 60°dislocations in {111} planes of the glide set [6]. These dislocations are dissociated into 30° and 90° Shockley partials with 1/6 $\langle 112\rangle$ Burgers vectors (two 30° partials for a screw, a 30° and a 90° partial for a 60° dislocation), separated by a stacking fault. Stacking faults are stable only in the glide set and the associated energies have been estimated in Si by first principles [241,242] in the range 38–75 mJ m^{-2}, leading to a large dissociation in the 4–8 nm range, consistent with experiments [243]. As a result, partial dislocations have been studied as isolated entities. With periodic boundary conditions, a dipole of partial dislocations with opposite Burgers vectors, bordered by a stacking fault, is introduced in the computational cell and does not recombine because of the high Peierls stress of the partials (see Sec. 6.3).

The 30° and 90° Shockley partial dislocations have been extensively studied by first principles, especially in Si. In contrast with the early assumption that dangling bonds are unavoidable in dislocation cores [250], LDA-DFT calculations [32] showed that an unreconstructed 90° partial dislocation is unstable and adopts an asymmetrical reconstruction without dangling bonds, shown in Fig. 23a. Later, a second core shown in Fig. 23b, with a double period reconstruction along the dislocation line, has been identified [244] and is of higher stability in most first-principles calculations. It is however currently admitted that both cores may coexist [251] because, as seen in Table 6, their energy difference is very small [245] and depends critically on the cell size and geometry [74] as well as on the boundary conditions and temperature [239]. We note that the reconstructions may adopt different variants, creating reconstruction defects along the dislocation lines [252]. The latter,

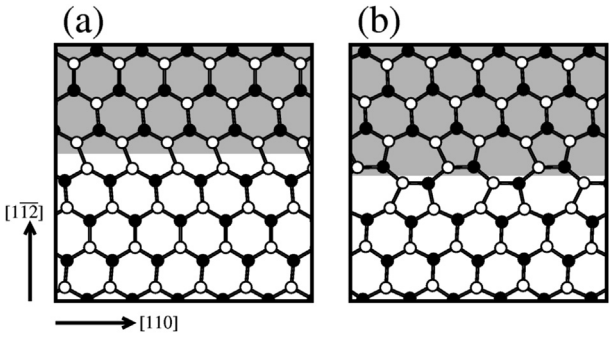

Fig. 23. Single- (a) and double-period (b) reconstructed cores of a 90° Shockley partial dislocation in Si. Reproduced with permission from Ref. [244].

Table 6
Energy differences between double- and single-period reconstructed 90° dislocation cores (in eV Å^{-1}) in different cubic semiconductors.

Ref.	Si	Diamond	Ge
[244]	−0.079		
[245]	−0.069	−0.235	−0.058
[74]	−0.011/+0.021		
[246]		[−0.069,−0.198]	
[247]	−0.05	−0.185	−0.04

Ref.	GaAs		SiC	
	Ga-core	As-core	Si-core	C-core
[247]	−0.01	+0.02	−0.09	−0.10
[248]	−0.01	+0.01		

illustrated in Fig. 24c and f, have been investigated by first principles [253,254] and are referred to as antiphase defects (APD), phase-switching defects or solitons [255].

The 90° partial dislocation has been studied in elemental semiconductors other than Si, in particular Ge and diamond. As seen in Table 6, Ge is very similar to Si, with an energy difference only slightly in favor of the double period core [245,247,256], while in diamond, this core is unambiguously more stable [246,256–259].

The 90° partial dislocation has also been investigated in cubic binary compounds, such as GaAs [247,260] and SiC [259,261,262]. In an AB compound, there are two inequivalent dislocation cores (except for the screw dislocation) with either A or B atoms predominant in the core. In the case of GaAs, energy differences between single and double period cores are negligible, for both the Ga- and As-rich 90° cores [247,260]. On the other hand, in SiC, the double period core is more stable for both the Si- and C-rich cores [259,262]. Beckman and Chrzan have shown that there is a relation between the relative stability of this core and the so-called Kleinman parameter, which quantifies the ease to bend or stretch atomic bonds in a zinc-blende structure [247].

Unlike the 90° Shockley partial, the 30° Shockley partial has a single stable structure [255] with a double period reconstruction shown in Fig. 24e, in both elemental and compound semiconductors [248,260,263]. The energy gain associated with the reconstruction ranges from 0.056 eV Å^{-1} to 0.119 eV Å^{-1} depending on the material (largest in Si, smallest for the As-core in GaAs).

Hexagonal semiconductors. Shockley partial dislocations also exist in wurtzite materials, along with several other types of partial dislocations [264]. In GaN for instance, the partials have a line along $[11\bar{2}0]$ with $1/3\,[1\bar{1}00]$ and $1/3\,[10\bar{1}0]$ Burgers vectors for 90° and 30° partials, respectively. The only reported first-principles calculation [265] showed that the reconstructed single period core is favored for both Ga- (by 0.14 eV Å^{-1}) and N-type (by 1.12 eV Å^{-1}) 90° partials compared to the unreconstructed core. However, to the best of our knowledge, the double period core has not been tested. For the 30° partial, the unreconstructed geometry is more stable by 0.002 eV Å^{-1} (0.4 eV Å^{-1}) for the Ga-core (N-core), in contrast with cubic systems. However, the very small energy difference for the Ga-core is probably strongly dependent on the details of the calculations, as for the 90° partial dislocation in Si [74].

6.2.2. Non-dissociated 1/2⟨110⟩ dislocations in cubic semiconductors

Cubic semiconductors. Below the BDT temperature, non-dissociated dislocations are observed in the shuffle set, with an 1/2⟨110⟩ Burgers vector and orientations including screw, 30°, and 41° [240,267]. Among these, only the non-dissociated screw dislocation has been investigated in Si using first principles [268]. A stable configuration in the glide set, the A core in Fig. 25, was found with the dislocation centered on a hexagon of the cubic diamond structure [269]. Later, a lower energy core (C_2, Fig. 25) was found [270], with a double period reconstruction along the line and a core centered on a glide set plane. Without reconstruction (C_1, Fig. 25), the screw dislocation is unstable [266].

The non-dissociated screw dislocation has received much less attention in semiconductors other than Si and several calculations (in Ge, 3C-SiC, GaAs, and diamond [258,271]) were performed before the discovery of the C_2 core. This core was however found most stable in SiC polytypes [272].

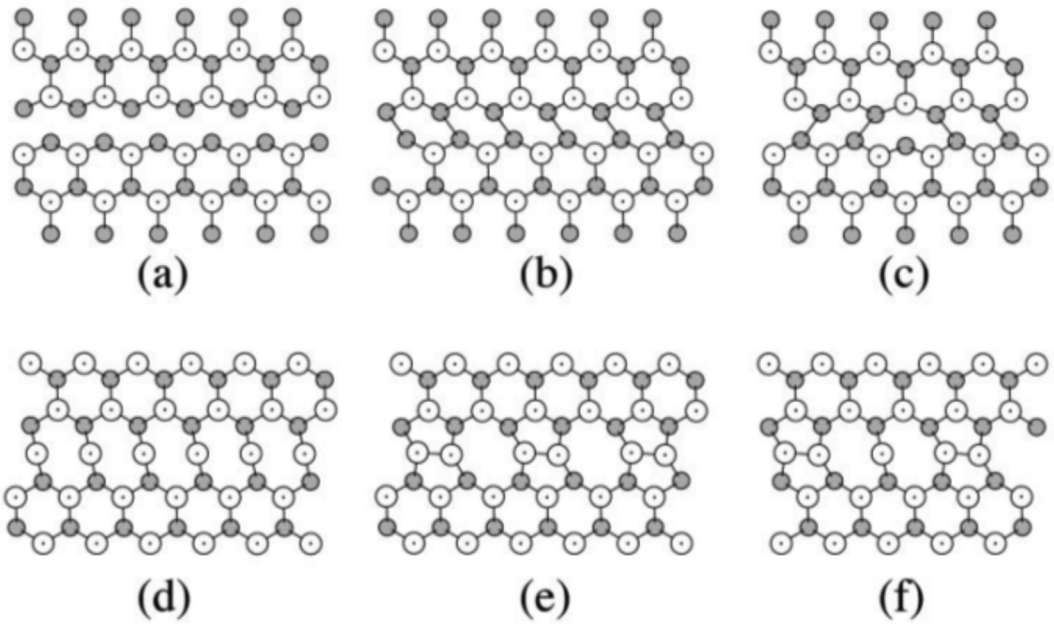

Fig. 24. Core structure of Shockley partial dislocations in the glide set of Si. For the 90° Schockley partial: (a) unreconstructed core, (b) reconstructed core, (c) Antiphase defect. Same for the 30° Schockley partial in (d,e,f). Reproduced with permission from Ref. [249].

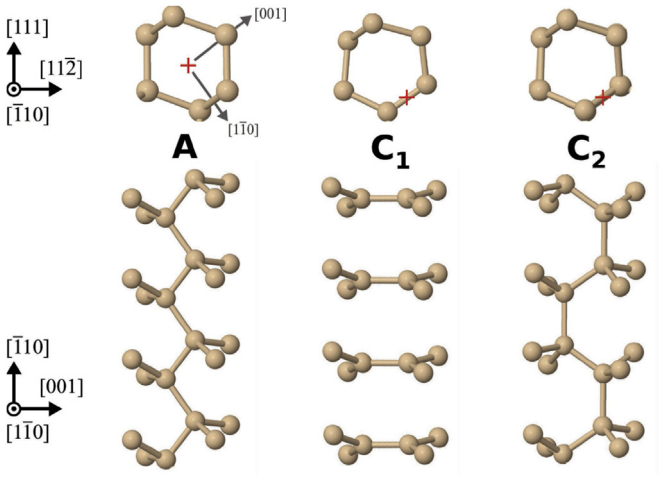

Fig. 25. Three possible core structures of a screw dislocation in the diamond cubic lattice. Reproduced with permission from Ref. [266].

Another important dislocation is the non-dissociated 60° dislocation, which plays a role in the relaxation of strained epitaxial films and in the plasticity of nano-objects [273,274]. As for the screw dislocation, different configurations are expected according to whether the core is in the glide or the shuffle set. Interatomic potential calculations predicted a fully-reconstructed compact core in the glide set (G core, Fig. 26) and dangling bonds in the shuffle set (S1 core, Fig. 26). With first principles in Si [275], the G core is the most stable and the S1 core is unstable and relaxes first to an open structure (S2 core, Fig. 26) and then to a stable configuration without dangling bonds (S3 core, Fig. 26). This core is however 0.156 eV Å^{-1} above the G core. The 60° dislocation in other cubic semiconductors has not been studied, except cubic GaN [276], where the glide G Ga-core and the shuffle S1 N-core were found stable, while the shuffle Ga-core relaxed to the S2 core.

Finally, we mention for the sake of exhaustivity perfect edge dislocations [277], which are not associated with plastic deformation but form at mismatched interfaces [278]. A stable and fully reconstructed core structure was found in the glide set, but to our knowledge, no other potential core geometries (such as a shuffle core) have been investigated so far.

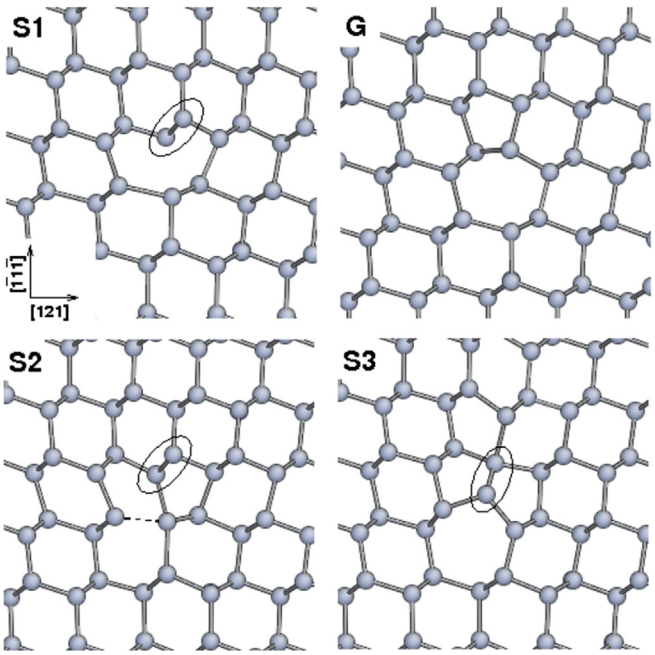

Fig. 26. Core structures for a non-dissociated 60° dislocation in a diamond cubic lattice. Reproduced with permission from Ref. [266].

Hexagonal semiconductors. The literature is much more limited and inconclusive concerning non-dissociated 1/3 ⟨2$\bar{1}\bar{1}$0⟩ in hexagonal wurtzite materials (equivalent to non-dissociated 1/2 ⟨110⟩ dislocations in cubic systems). Apparently, only interatomic potentials [279] and tight-binding calculations [280,281] in GaN have been reported, indicating that the basal screw dislocation in the glide C_1 configuration is more stable than the shuffle A core [280]. For the 60° basal dislocation, the most stable N-core has the glide G geometry, while for the Ga-core, the lowest energy was found for a shuffle configuration [281].

6.2.3. *Prismatic dislocations in wurtzite semiconductors*

Prismatic dislocations form another important type of dislocations in semiconductors. They have mostly been studied in GaN and are usually called threading dislocations because they relax the misfit strain during ⟨0001⟩ film growth [282]. Three different characters have been reported: screw with a ⟨*c*⟩ Burgers vector along ⟨0001⟩, mixed with a ⟨*c*+*c*⟩ Burgers vector along 1/3 ⟨1$\bar{2}$13⟩, and edge with a ⟨*a*⟩ Burgers vector along 1/3 ⟨1$\bar{2}$10⟩.

In the first core considered for a screw dislocation [284], named 'A full core', the dislocation line was located at the centre of a hexagon in the basal plane (see Fig. 27a). This configuration is stable, but its energy can be reduced by 0.33 eV Å^{-1} if both Ga and N atoms are removed from the central hexagon (Figs. 27b and 28). The resulting 'A open core' has an internal free surface but avoids the severely stretched and bent bonds found for the A full core. Moreover, it is energetically favorable to remove N atoms from the

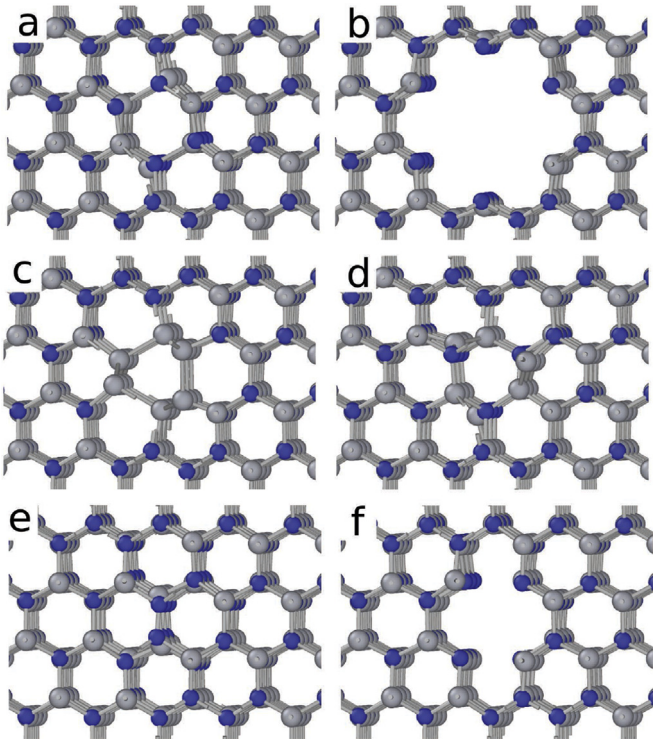

Fig. 27. Core structures of a prismatic screw dislocation in GaN: (a) A full core, (b) A open core, (c) A Ga-filled, (d) A N-half filled, (e) B full core, (f) B open core. Ga atoms are in grey, N atoms in blue. (For interpretation of the references to colour in this figure legend, the reader is referred to the web version of this article.)

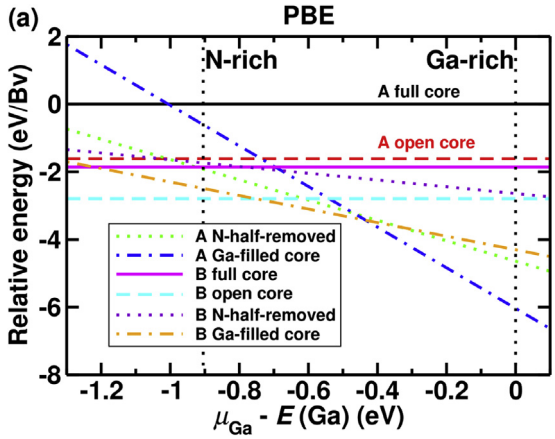

Fig. 28. Excess energies for several prismatic screw dislocation configurations in GaN, relative to the A full core as a function of the Ga chemical potential. Reproduced with permission from Ref. [283].

core [285] (Fig. 27c) rather than Ga atoms because the resulting non-stoichiometric configuration, called 'A Ga-filled' core, is 0.37 eV Å^{-1} below the A open core (Fig. 28) in Ga-rich conditions (i.e. when the Ga chemical potential equals that of the bulk). In N-rich condition, another core, in which only half of the N core atoms are removed, is most stable [286] ('A N-half filled' core, Fig. 27d). Also, a stoichiometric 'B full core' (Fig. 27e), where the dislocation line is shifted to the edge of a basal hexagon was found more stable than the A open core [287] and is also probably more stable than the N half-filled core. Nevertheless, a new configuration, the 'B open core', was found recently with both Ga and N core atoms removed (Fig. 27e), with the lowest excess energy in N-rich conditions (Fig. 28) [283]. We note that this last work was the first to employ a hybrid exchange-correlation functional, going beyond the usual local density and generalized gradient approximations.

Concerning edge dislocations in GaN [284], a stoichiometric core was first proposed with an 8-atom ring (Fig. 29a). Later, a deficit of Ga or N atoms in the core was found energetically favorable,

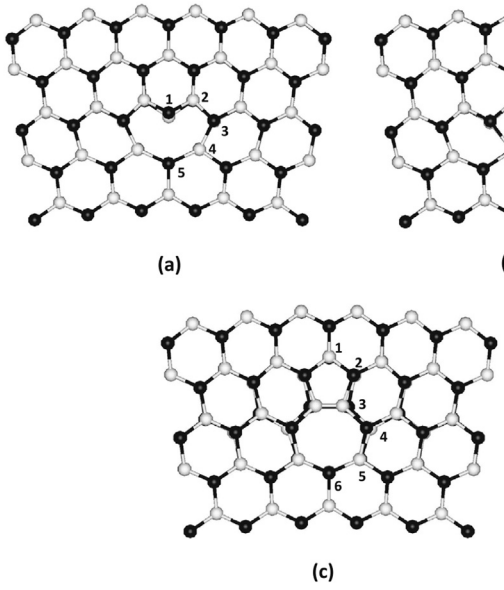

Fig. 29. Core structures of a prismatic edge dislocation in a wurtzite material: (a) 8-atom ring core, (b) 4-atom ring core, (c) 5/7-atom ring core. Reproduced with permission from Ref. [288].

depending on the growth conditions and the Fermi level [289]. This last point is important since most of the available theoretical investigations do not consider how doping may influence core stability. Considering charged cells is difficult with periodic boundary conditions due to the resulting long-range electrostatic interactions, although several correction schemes have been proposed [290]. The resulting substoichiometric structure is referred to as 5/7-atom ring or open core (Fig. 29c). Also, a combined TEM/first principles investigation suggested that a third core, stoichiometric with a central 4-atom ring (Fig. 29b), should also be considered [291]. Despite being experimentally detected, this configuration is about 0.13 eV Å^{-1} above the 5/7-atom ring geometry. This stability is reversed in presence of an applied tensile strain of 2%, but the difference is small (~0.05 eV Å^{-1}). As a consequence, it is currently accepted that all three configurations in Fig. 29 may exist in GaN. The same conclusion applies to AlN [292] and InN [293].

6.2.4. *Interaction with impurities and point defects*

The segregation of impurities at dislocation cores is in most cases energetically favorable in semiconductors. One reason is that, because bonds are strongly distorted in dislocation cores, there are many potential inequivalent sites for substitutional and interstitial impurities with different bonding environments. An impurity then usually finds a site with an appropriate local volume or electronic structure with a reduced energy compared to the bulk. For instance, segregation energies in the range 0–0.7 eV were found in Si for the usual substitutional dopants (B, N, P, As) in the 90° Shockley partial core [294–297]. In the specific case of As, segregation energies of 0.18 eV for a 30° partial dislocation [298] and 0.25 eV for a perfect edge dislocation [299] were also obtained.

In cubic SiC, different impurities have been considered: Al and P substituting Si, and B and N substituting C, in interaction with the C- and the Si-core of a 30° partial dislocation [301]. It was found that (i) Al segregates to the Si-core (0.95 eV) but not to the C-core (−0.15 eV) (ii) P segregates to both Si- (0.6 eV) and C-cores (0.15 eV) (iii) B also segregates to both Si- (0.7 eV) and C-cores (1.55 eV) (iv) N segregates to the C-core (0.55 eV) but not to the Si-core (−0.2 eV). These results clearly show that it is not possible to predict with simple arguments how an impurity interacts with a dislocation core.

The situation is even more complex with interstitial impurities because of the larger number of potential occupancy sites, but segregation is also usually favorable. For instance, in the case of atomic H and molecular H_2 in Si, the largest segregation energies were found from 0.69 eV to 1.28 eV for H, and from 0.78 eV to 1.13 eV for H_2 depending on the dislocation core [302,303]. A similar result was obtained for a 90° partial dislocation in diamond [304]. Finally, as illustrated in Fig. 30, segregation energies from 0.1 eV to 0.62 eV were recently found for interstitial Fe impurities interacting with Shockley partial dislocations in Si [300].

In addition to impurities, point defects like vacancies and interstitials may also affect dislocation cores, as attested by several experimental works [305,306]. Interstitials and vacancies may activate climb, modify the structure of the core or of the kinks, and alter the electronic properties. Surprisingly, only few first-principles studies were dedicated to this issue. Large binding energies were found between vacancies and Shockley partials in Si (2.0 eV and 0.9 eV for the 90° and 30° partial respectively) [307], showing that these dislocations may be efficient sinks for point defects. Also, Justo et al. [308] examined whether partial dislocations could be moved to a shuffle plane as a result of a core transformation induced by vacancies. However, they concluded that this transformation could only occur in non-equilibrium conditions, such as a vacancy supersaturation. Regarding interstitials, no work has been reported to our knowledge.

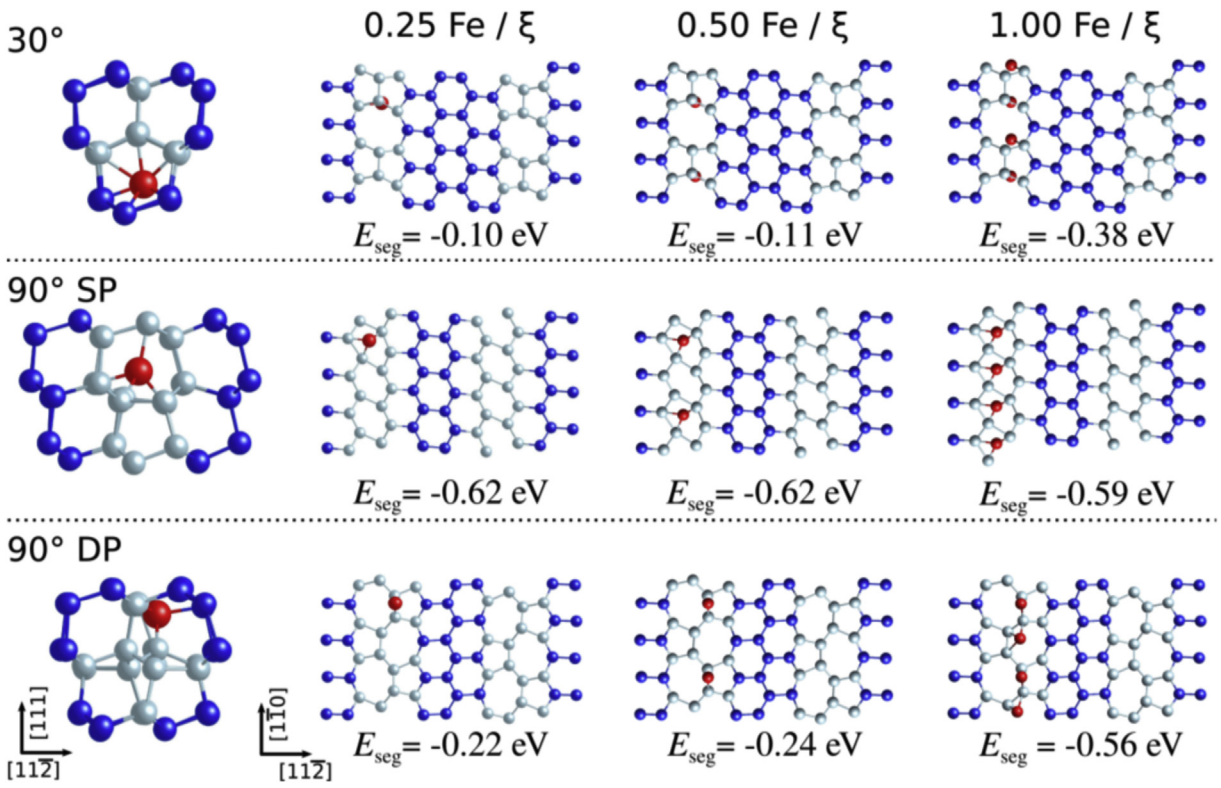

Fig. 30. Atomic structures of the most stable configurations of Fe impurities (red spheres) segregated in different Schockley partial cores in Si. The left column shows the location of a single Fe atom viewed along the dislocation line. The other columns show the location of the Fe atoms from a top view for increasing Fe concentrations. Si atoms are in blue, with light blue atoms inside the dislocation cores. Reproduced with permission from Ref. [300]. (For interpretation of the references to colour in this figure legend, the reader is referred to the web version of this article.)

The aggregation of impurities in dislocation cores greatly depends on the dislocation core. In Si, aggregation is energetically favored in the case of substitutional As atoms in a 90° partial [296], but not in a 30° partial [309]. A similar result was obtained for interstitial Fe atoms in Si, aggregation being predicted in the 90° partial with a double period reconstruction, but not with a single period [300]. First-principles calculations also showed that H aggregation in Shockley partial dislocations is energetically favored in Si, with a predicted maximum concentration of 1.3–1.56 H/Å along the dislocation line, depending on the dislocation core [303]. Moreover, as in BCC metals (see Sec. 4.5), impurities can significantly alter the dislocation core structure. For instance, H promotes the breaking of weak, highly stretched or bent bonds, thus leading to a local deconstruction of the dislocation core. Similar cases were reported in the case of N in SiC [301] and H in diamond [304].

6.3. Mobility

Peierls valleys in semiconductors are quite deep, leading to high Peierls stresses and limited mobilities at low temperatures, resulting in brittleness below the BDT temperature. At higher temperatures, lower stresses are needed, and dislocation glide involves the nucleation and migration of kinks along the dislocation lines [6].

6.3.1. Peierls stress

The Peierls stress of non-dissociated screw dislocations, which govern plasticity at low temperatures, has been determined in Si from first principles. For the A core (see Fig. 25), while the first calculations yielded unrealistically large values (22–46 GPa) [310], more recent calculations found 4.2 ± 0.3 GPa [62]. In this work, the effect of the boundary conditions was corrected using elasticity theory. This value was later confirmed, estimating the Peierls stress from the maximum slope of the Peierls barrier obtained with NEB method [83].

Regarding the most stable screw core (C_2 core in Fig. 25), a Peierls stress of 6 GPa was found [270], hinting that this core may be less mobile than the A core. In SiC polytypes, the Peierls stress of the A core was found from 8.9 GPa to 10.2 GPa, depending on the polytype and glide direction [272].

The case of the non-dissociated 60° dislocation is peculiar because first-principles calculations suggest that both stable cores (G and S3 cores in Fig. 26) are sessile, while the transient S1 shuffle core is mobile, with a Peierls stress between 1.1 and 2.8 GPa [275]. This result is consistent with investigations of dislocation nucleation in Si, demonstrating the formation and propagation of the S1 dislocation core from a surface [311].

6.3.2. Peierls-Nabarro model

At the time when a direct determination of the Peierls stress from first principles was out-of-reach, several attempts were made using the Peierls-Nabarro model [312], with GSFE surfaces computed *ab initio*, as in FCC metals (see Sec. 3). However, despite proposed improvements [49], the Peierls stresses thus obtained (for instance, 7.3 GPa and 9.9 GPa for the non-dissociated 60° and screw dislocations in Si [313]) are much larger than with full DFT. This is probably because dislocation cores in semiconductors are narrow and include reconstructed bonds that can not be described within the PN model.

6.3.3. Kink formation and migration

Much effort has been devoted to determine the formation and

migration energies of kinks on Shockley partial dislocations in Si, first using interatomic potentials and the tight-binding theory [255,315,316] and later using DFT.

The kink migration energy on a 30° glide Shockley partial was estimated at 2.1 eV [317]. On 90° partials with a single period reconstruction, the single kink formation and migration energies were estimated at 0.1 and 1.8 eV, respectively [318]. Other works found similar low formation energies (0.04 eV, 0.16 eV [319,320]), but a lower migration energy (1.09 eV). These values do not agree with the commonly accepted experimental values, 0.4–0.7 eV and 1.2 eV for the formation and migration energies of isolated kinks, respectively. One straightforward explanation lies in the difficulty to make accurate kink models using small DFT simulation cells. Also, several kink configurations are possible for a given dislocation core. Taking into account reconstruction defects along the dislocation lines and their interactions with kinks, we are left with a large variety of possible configurations, which has been qualified as 'bottomless complexity' by Bulatov [321].

Kinks on single period 90° cores have also been investigated in AB compounds. The 'bottomless complexity' is then twice worse, because both A- and B-type partial cores have to be considered. In GaAs, kink formation energies were estimated at 0.07 eV (As-core) and 0.27 eV (Ga-core) and migration energies at 0.7 eV (As-core) and 1.1 eV (Ga-core) [318]. In 3C-SiC, the formation energies for the Si- and C-cores are 0.1 eV and 0.3 eV, while the migration energies are 2.7 eV and 1.4 eV, respectively [261].

Much less attention has been devoted to kinks on perfect dislocations, probably because there are no available experimental data for comparison. However, a single kink configuration was found on a Si screw dislocation with an A core [314,322], with a large formation energy (1.36 eV) and a low migration energy (below 0.05 eV), as illustrated in Fig. 31. This is in stark contrast with kinks on partial dislocations discussed above.

6.3.4. *Influence of defects*

Point defects in semiconductors can affect dislocation mobility in a number of ways besides climb [308]. For instance, the Fermi level can be shifted due to the presence of doping impurities, which in turn can modify the energetics of kinks. Also, impurities segregated in dislocation cores can either provide an additional barrier to dislocation motion or conversely, enhance dislocation mobility. Many experimental data are available [323], but there is a critical lack of theoretical investigations. To our knowledge, only the influence of H on the mobility of a 90° partial dislocation in Si was studied [324], finding an increased mobility as in diamond [325].

6.3.5. *Effect of pressure*

As mentioned above, dislocations are observed in the brittle regime in cases of confined plasticity [240] and in micro-pillars [326,274]. This raises the question of the influence of pressure on dislocation mobility, an issue largely neglected in previous works. To our knowledge, only the case of a shuffle screw dislocation in Si has been considered [327]. It was found that an applied compressive pressure decreases the Peierls barrier in the shuffle plane and increases the barrier in the {100} plane. This work highlights that plasticity in semiconductors can not be described by a simple Schmid criterion, and that applied stresses should be taken into account in the analysis of experimental results.

7. Conclusions and perspectives

This overview article highlights the extreme diversity and richness of dislocation core structures in metals and semiconductors. *Ab initio* calculations have served these past few years to identify many new stable and metastable cores in pure metals

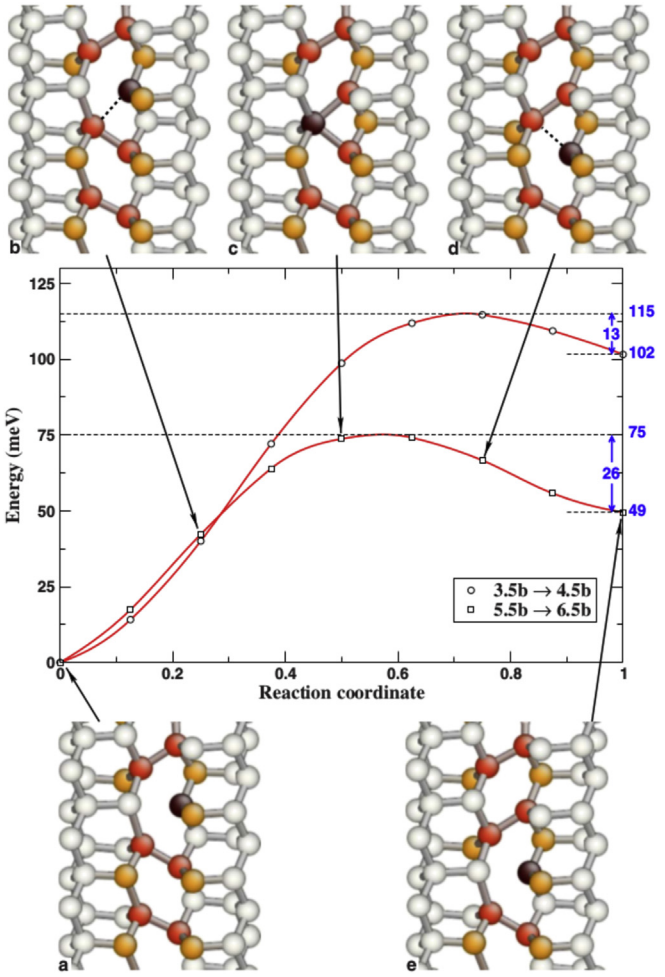

Fig. 31. Migration barrier computed with NEB for a kink on a non-dissociated dislocation in Si. The initial and final energies are different because the distance between kinks varies, from 3.5 to 4.5b (resp. 5.5–6.5b) for the upper (resp. lower) curve. The insets show the dislocation line along a $[1\bar{2}1]$ projection. Reproduced with permission from Ref. [314].

(*e.g.* planar, non-planar and compact prismatic cores in HCP metals), in alloys (*e.g.* the polarized core in W-Re and the reconstructed hard core in BCC Fe(C)) and semiconductors (*e.g.* the B open core in GaN). These cores involve complex reconstructions and stacking faults that can be reliably predicted only using electronic-level calculations. We note however that in most cases, the stability of these structures is a numerical evidence and remains to be explained based on simple physical arguments.

The obvious main limitation of *ab initio* calculations is the number of atoms that can be simulated, which is particularly limited in metals. As a result, even using flexible boundary conditions to mimic infinite lateral dimensions, the geometries considered so far have been restricted in metals to straight infinite periodic dislocations. For periodic boundary conditions, it should be possible to divide by two the number of atoms and to include a single dislocation in the simulation cell by using anti-periodic boundary conditions, a solution already proposed for the modeling of grain boundaries [328]. *Ab initio* calculations using such boundary conditions would require to implement generalized Bloch functions as currently done to model spin waves in magnetic materials [329].

Not being able to include kinks on high Peierls stress dislocations, or jogs, effectively limits the predictions of the calculations to

0 K. Moreover, in this limit, quantum effects including tunneling [330] and zero-point energy vibrations [151] have been shown to impact dislocation glide. However, correcting for these effects remains computationally expensive and has not been done so far.

To access finite temperatures, *ab initio* calculations have been used to compute characteristic energies, like core energies, Peierls barriers, kink energies (in semiconductors only), that enter higher-scale models of dislocation energetics. An example already mentioned is the line tension model [156], which includes curvature, and can in turn be used in thermally-activated models of mobility. Kink formation energies have been computed in semiconductors where simulation cells are large enough, but it is still out of reach in metals. A direct calculation for instance of a kink-pair formation energy would allow for a more quantitative prediction of finite-temperature dislocation mobility and would open the door to many other processes, such as chemical effects on kink formation and propagation that may also affect dislocation mobility.

Also, to address finite temperature properties, free energies should be computed instead of energies. An attempt was done in semiconductors [239]. In BCC metals, free energy Peierls potentials were shown to vanish rapidly with temperature, implying a stronger temperature-dependence of dislocation mobility than expected from Peierls energies [331]. However, these calculations were performed with an interatomic potential and a confirmation and generalization of free energies calculations with *ab initio* calculations would be highly valuable to faithfully predict finite-temperature properties. More generally, the influence of local composition on dislocation cores illustrated here in both BCC metals and compound semiconductors highlights the need to search for core structures of minimal free energy in the grand canonical ensemble.

Another challenge related to the small length of dislocation accessible to *ab initio* calculations is that, when studying chemical effects, *e.g.* the interaction of solute atoms with a dislocation, the calculations are restricted to the high-concentration regime. Then remain questions such as: what is the critical local concentration of O atoms on a screw $\langle a \rangle$ dislocation in HCP Zr to induce the cross-slipped structure of Fig. 17b? Theories have been developed to assert the effect of solute atoms on dislocation mobility using *ab initio* interaction energies. The latter are reviewed in the companion overview paper by Varvenne et al. [332], but direct calculations to address concentration regimes of core reconstructions would be particularly interesting. Also, energy pathways associated with solute diffusion near (segregation) and inside (pipe diffusion) dislocation cores are highly desirable since in this region, neither elasticity nor interatomic potentials are reliable. Similarly, the study of the effect of chemistry on dislocation cores has started only recently, but should be extended for instance to intermetallics and compounds. In addition, in semiconductors, the effect of doping and charge carrier recombination at dislocation cores and kinks are other processes that may affect dislocation mobility and should be analyzed using first principles.

An important direction to extend the size of the simulation cells is the development of approximate but reliable schemes to determine electronic structures. Orbital-free DFT is an example mentioned above [118,195], and tight-binding DFT is another [333]. Bond-order [145], ReaxFF [334] or charge-optimized many-body [335,336] potentials may also be interesting trade-offs between realism and computational cost.

Another important perspective concerns calculations under finite strains or stresses. Most calculations so far have considered dislocations under either no or simple stress geometries, mainly simple shear. However, non-Schmid effects related to shear stresses resolved perpendicularly to the Burgers vector are known to affect dislocation glide in FCC metals (Escaig stresses on cross-slip [337]), BCC metals (non-glide effects [23]) and semiconductors [338]. As mentioned above, the pressure was also shown to affect dislocations in semiconductors. Non-glide stresses are particularly important in the small-scale plasticity of nanostructures where very large stresses, exceeding the GPa, are reached [339,340] and may strongly affect dislocation core structures and properties.

Finally, there has been recently a convergence between experimental techniques and simulations, with for instance aberration-corrected electron microscopy allowing to visualize solute segregation inside a dislocation core [201]. However, many of the new core structures predicted *ab initio* are to be confirmed experimentally and conversely, many experimental observations should be explained at the atomic scale, like the jerky motion observed at low temperature in BCC metals [122]. These are exciting perspectives that remain to be explored.

Acknowledgements

Sandrine Brochard, Nermine Chaari, Lucile Dezerald, Julien Godet, Bérengère Lüthi and Laurent Proville are acknowledged for their important contributions to the works presented here. DR acknowledges support from LABEX iMUST (ANR-10-LABX-0064) of Université de Lyon (program "Investissements d'Avenir", ANR-11-IDEX-0007) and the Institut Universitaire de France. Part of this work was performed using HPC resources from GENCI-CINES and -TGCC (grant 2016-096847). EC also acknowledges PRACE for access to the Curie resources based in France at TGCC (project PlasTitZir2).

References

[1] M.S. Duesbery, The influence of core structure on dislocation mobility, Philos. Mag. 19 (1969) 501–526.
[2] P. Veyssière, Dislocation core effects in plasticity, Rev. Phys. Appl. (Paris) 23 (1988) 431–443.
[3] W. Cai, V.V. Bulatov, J. Chang, J. Li, S. Yip, Dislocation core effects on mobility, in: F.R.N. Nabarro, J.P. Hirth (Eds.), Dislocations in Solids, vol. 12, Elsevier, 2004, pp. 1–80.
[4] V. Vitek, V. Paidar, Non-planar dislocation cores: a ubiquitous phenomenon affecting mechanical properties of crystalline materials, in: J.P. Hirth (Ed.), Dislocations in Solids, vol. 14, Elsevier, 2008, pp. 439–514.
[5] L. Kubin, Dislocations, Mesoscale Simulations and Plastic Flow, Oxford University Press, 2013.
[6] J.P. Hirth, J. Lothe, Theory of Dislocations, Wiley, New-York, 1982.
[7] D.J. Bacon, D.M. Barnett, R.O. Scattergood, Anisotropic continuum theory of lattice defects, Prog. Mater. Sci. 23 (1980) 51–262.
[8] V.L. Indenbom, J. Lothe (Eds.), Elastic Strain Fields and Dislocation Mobility, Modern Problems in Condensed Matter Sciences, vol. 31, 1992. North-Holland, Amsterdam.
[9] R. Peierls, The size of a dislocation, Proc. Phys. Soc. 52 (1940) 34–37.
[10] F.R.N. Nabarro, Dislocations in a simple cubic lattice, Proc. Phys. Soc. 59 (1947) 256–272.
[11] V.V. Bulatov, W. Cai, Computer Simulations of Dislocations, Oxford University Press, New-York, 2006.
[12] R.M.J. Cotterill, M. Doyama, The energy and atomic configuration of a screw dislocation in an FCC metal, Phys. Lett. 14 (1965) 79–80.
[13] R.M.J. Cotterill, M. Doyama, Energy and atomic configuration of complete and dissociated dislocations. I. Edge dislocation in an FCC metal, Phys. Rev. 145 (1966) 465–478.
[14] M. Doyama, R.M.J. Cotterill, Energy and atomic configurations of complete and dissociated dislocations. II. Screw dislocation in an FCC metal, Phys. Rev. 150 (1966) 448–455.
[15] R. Chang, L.J. Graham, Edge dislocation core structure and Peierls barrier in body-centered cubic iron, Phys. Stat. Sol. 18 (1966) 99–103.
[16] R. Chang, Screw dislocation core structure in body-centred cubic iron, Philos. Mag. 16 (1967) 1021–1029.
[17] V. Vitek, Theory of the core structures of dislocations in body-centered-cubic metals, Cryst. Latt. Def. 5 (1974) 1–34.
[18] M.P. Puls, M.J. Norgett, Atomistic calculation of the core structure and Peierls energy of an (a/2)[110] edge dislocation in MgO, J. Appl. Phys. 47 (1976) 466–477.
[19] R.G. Hoagland, J.P. Hirth, P.C. Gehlen, Atomic simulation of the dislocation core structure and Peierls stress in alkali halide, Philos. Mag. 34 (1976) 413–439.
[20] D.J. Bacon, J.W. Martin, The atomic structure of dislocations in hcp metals I.

Potentials and unstressed crystals, Philos. Mag. A 43 (1981) 883–900.
[21] M.S. Duesbery, B. Joos, D.J. Michel, Dislocation core studies in empirical silicon models, Phys. Rev. B 43 (1991) 5143–5146.
[22] R. Pasianot, D. Farkas, E.J. Savino, Dislocation core structure in ordered intermetallic alloys, J. Phys. III 1 (1991) 997–1014.
[23] M.S. Duesbery, V. Vitek, Plastic anisotropy in b.c.c. transition metals, Acta Mater. 46 (1998) 1481–1492.
[24] J.A. Moriarty, J.F. Belak, R.E. Rudd, P. Söderlind, F.H. Streitz, L.H. Yang, Quantum-based atomistic simulation of materials properties in transition metals, J. Phys. Condens. Matter 14 (2002) 2825–2857.
[25] S. Takeuchi, Core structure of a screw dislocation in the b.c.c. lattice and its relation to slip behaviour of α-iron, Philos. Mag. A 39 (1979) 661–671.
[26] V. Vitek, M. Mrovec, J.L. Bassani, Influence of non-glide stresses on plastic flow: from atomistic to continuum modeling, Mater. Sci. Eng. A 365 (2004) 31–37.
[27] R. Gröger, V. Vitek, Directional versus central-force bonding in studies of the structure and glide of 1/2 ⟨111⟩ screw dislocations in bcc transition metals, Philos. Mag. 89 (2009) 3163–3178.
[28] S. Chiesa, M.R. Gilbert, S.L. Dudarev, P.M. Derlet, H. Van Swygenhoven, The non-degenerate core structure of a ⟨111⟩ screw dislocation in bcc transition metals modelled using Finnis-Sinclair potentials: The necessary and sufficient conditions, Philos. Mag. 89 (2009) 3235–3243.
[29] C. Woodward, First-principles simulations of dislocation cores, Mater. Sci. Eng. A 400–401 (2005) 59–67.
[30] M.I. Heggie, R. Jones, G. Lister, A. Umerski, Structure and properties of dislocations, Inst. Phys. Bristol Conf. Ser. 104 (1989) 43–46.
[31] M. Heggie, R. Jones, A. Umerski, Interaction of impurities with dislocation cores in silicon, Philos. Mag. A 63 (1991) 571–584.
[32] J.R.K. Bigger, D.A. McInnes, A.P. Sutton, M.C. Payne, I. Stich, R.D. King-Smith, D.M. Bird, L.J. Clarke, Atomic and electronic structures of the 90° partial dislocation in silicon, Phys. Rev. Lett. 69 (1992) 2224–2227.
[33] S. Ismail-Beigi, T.A. Arias, Ab initio study of screw dislocations in Mo and Ta: a new picture of plasticity in bcc transition metals, Phys. Rev. Lett. 84 (2000) 1499–1502.
[34] C. Domain, A. Legris, Atomic scale simulation of the effect of hydrogen on dislocations in Zr, in: Mater. Res. Soc. Symp. Proc., vol. 653, 2000, p. Z3.8.
[35] F. Ferrer, A. Barbu, T. Bretheau, J. Crépin, F. Willaime, D. Charquet, The effect of small concentrations of sulfur on the plasticity of zirconium alloys at intermediate temperatures, in: G.D. Moan, P. Rudling (Eds.), Zirconium in the Nuclear Industry: Thirteenth International Symposium vol. 1423, American Society for Testing and Materials Special Technical Publication, W Conshohocken, USA, 2002, pp. 863–885. American Society Testing and Materials.
[36] C. Woodward, D.R. Trinkle, L.G. Hector Jr., D.L. Olmsted, Prediction of dislocation cores in aluminum from density functional theory, Phys. Rev. Lett. 100 (2008) 045507–045510.
[37] C. Woodward, S.I. Rao, Ab-Initio simulation of isolated screw dislocations in BCC Mo and Ta, Philos. Mag. A 81 (2001) 1305–1316.
[38] G. Lu, E.B. Tadmor, E. Kaxiras, From electrons to finite elements: a concurrent multiscale approach for metals, Phys. Rev. B 73 (2006) 024108–024111.
[39] Y. Liu, G. Lu, Z. Chen, N. Kioussis, An improved QM/MM approach for metals, Model. Simul. Mater. Sci. Eng. 15 (2007) 275–284.
[40] W. Cai, V.V. Bulatov, J. Chang, J. Li, S. Yip, Anisotropic elastic interactions of a periodic dislocation array, Phys. Rev. Lett. 86 (2001) 5727–5730.
[41] W. Cai, V.V. Bulatov, J. Chang, J. Li, S. Yip, Periodic image effects in dislocation modelling, Philos. Mag. 83 (2003) 539–567.
[42] J. Hafner, Ab-initio simulations of materials using VASP: density-functional theory and beyond, J. Comp. Chem. 29 (2008) 2044–2078.
[43] P. Giannozzi, S. Baroni, N. Bonini, M. Calandra, R. Car, C. Cavazzoni, D. Ceresoli, G.L. Chiarotti, M. Cococcioni, I. Dabo, A. Dal Corso, S. de Gironcoli, S. Fabris, G. Fratesi, R. Gebauer, U. Gerstmann, C. Gougoussis, A. Kokalj, M. Lazzeri, L. Martin-Samos, N. Marzari, F. Mauri, R. Mazzarello, S. Paolini, A. Pasquarello, L. Paulatto, C. Sbraccia, S. Scandolo, G. Sclauzero, A.P. Seitsonen, A. Smogunov, P. Umari, R.M. Wentzcovitch, QUANTUM ESPRESSO: A modular and open-source software project for quantum simulations of materials, J. Phys. Condens. Matter 21 (2009) 395502–395520.
[44] J.M. Soler, E. Artacho, J.D. Gale, A. García, J. Junquera, P. Ordejón, D. Sánchez-Portal, The SIESTA method for ab initio order-N materials simulation, J. Phys. Condens. Matter 14 (2002) 2745–2779.
[45] X. Gonze, B. Amadon, P.M. Anglade, J.M. Beuken, F. Bottin, P. Boulanger, F. Bruneval, D. Caliste, R. Caracas, M. Côté, T. Deutsch, L. Genovese, P. Ghosez, M. Giantomassi, S. Goedecker, D.R. Hamann, P. Hermet, F. Jollet, G. Jomard, S. Leroux, M. Mancini, S. Mazevet, M.J.T. Oliveira, G. Onida, Y. Pouillon, T. Rangel, G.M. Rignanese, D. Sangalli, R. Shaltaf, M. Torrent, M.J. Verstraete, G. Zerah, J.W. Zwanziger, ABINIT: first-principles approach to material and nanosystem properties, Comput. Phys. Commun. 180 (2009) 2582–2615.
[46] V. Vitek, Intrinsic stacking faults in body-centred cubic crystals, Philos. Mag. 18 (1968) 773–786.
[47] V.V. Bulatov, E. Kaxiras, Semidiscrete variational Peierls framework for dislocation core properties, Phys. Rev. Lett. 78 (1997) 4221–4224.
[48] S. Ogata, J. Li, S. Yip, Ideal pure shear strength of aluminum and copper, Science 298 (2002) 807–811.
[49] B. Joós, M.S. Duesbery, The Peierls stress of dislocations: an analytical formula, Phys. Rev. Lett. 78 (1997) 266–269.
[50] D. Ferre, P. Carrez, P. Cordier, Modeling dislocation cores in $SrTiO_3$ using the Peierls-Nabarro model, Phys. Rev. B 77 (2008) 014106.
[51] K. Gouriet, P. Carrez, P. Cordier, A. Guitton, A. Joulain, L. Thilly, C. Tromas, Dislocation modelling in Ti_2 AlN MAX phase based on the Peierls-Nabarro model, Philos. Mag. 95 (2015) 2539–2552.
[52] M. Benoit, N. Tarrat, J. Morillo, Density functional theory investigations of titanium γ-surfaces and stacking faults, Model. Simul. Mater. Sci. Eng. 21 (2013) 015009.
[53] J.R. Morris, Y.Y. Ye, K.M. Ho, C.T. Chan, M.H. Yoo, Structures and energies of compression twin boundaries in hcp Ti and Zr, Philos. Mag. A 72 (1995) 751–763.
[54] G. Henkelman, G. Jóhannesson, H. Jónsson, Methods for finding saddle points and minimum energy paths: theoretical methods in condensed phase chemistry, in: S.D. Schwartz (Ed.), Progress in Theoretical Chemistry and Physics, vol. 5, Springer, Netherlands, 2000, pp. 269–302.
[55] P. Kwaśniak, P. Śpiewak, H. Garbacz, K.J. Kurzydłowski, Plasticity of hexagonal systems: split slip modes and inverse Peierls relation in α-Ti, Phys. Rev. B 89 (2014) 144105–144110.
[56] N. Garvik, P. Carrez, S. Garruchet, P. Cordier, Numerical modeling of the core structure of [100] dislocations in Fe_3C cementite, Scr. Mater. 99 (2015) 61–64.
[57] A.N. Stroh, Dislocations and cracks in anisotropic elasticity, Philos. Mag. 3 (1958) 625–646.
[58] A.N. Stroh, Steady state problems in anisotropic elasticity, J. Math. Phys. (Cambridge, Mass.) 41 (1962) 77–103.
[59] J.D. Eshelby, W.T. Read, W. Shockley, Anisotropic elasticity with applications to dislocation theory, Acta Metall. 1 (1953) 251–259.
[60] E. Clouet, L. Ventelon, F. Willaime, Dislocation core energies and core fields from first principles, Phys. Rev. Lett. 102 (2009) 055502–055505.
[61] V.B. Shenoy, R. Phillips, Finite-sized atomistic simulations of screw dislocations, Philos. Mag. A 76 (1997) 367–385.
[62] L. Pizzagalli, P. Beauchamp, First principles determination of the Peierls stress of the shuffle screw dislocation in silicon, Philos. Mag. Lett. 84 (2004) 729–736.
[63] J.E. Sinclair, P.C. Gehlen, R.G. Hoagland, J.P. Hirth, Flexible boundary conditions and nonlinear geometric effects in atomic dislocation modeling, J. Appl. Phys. 49 (1978) 3890–3897.
[64] Z. Chen, G. Lu, N. Kioussis, N. Ghoniem, Effect of the local environment on the mobility of dislocations in refractory bcc metals: concurrent multiscale approach, Phys. Rev. B 78 (2008) 134102–134106.
[65] D.R. Trinkle, Lattice Green function for extended defect calculations: computation and error estimation with long-range forces, Phys. Rev. B 78 (2008) 014110–014120.
[66] M. Ghazisaeidi, D.R. Trinkle, Convergence rate for numerical computation of the lattice Green's function, Phys. Rev. E 79 (2009) 037701–037704.
[67] J.A. Yasi, D.R. Trinkle, Direct calculation of the lattice Green function with arbitrary interactions for general crystals, Phys. Rev. E 85 (2012) 066706–066714.
[68] S. Rao, C. Hernandez, J.P. Simmons, T.A. Parthasarathy, C. Woodward, Green's function boundary conditions in two-dimensional and three-dimensional atomistic simulations of dislocations, Philos. Mag. A 77 (1998) 231–256.
[69] C. Woodward, S.I. Rao, Flexible ab initio boundary conditions: simulating isolated dislocations in bcc Mo and Ta, Phys. Rev. Lett. 88 (2002) 216402–216405.
[70] D.E. Segall, A. Strachan, W.A. Goddard III, S. Ismail-Beigi, T.A. Arias, Ab Initio and finite-temperature molecular dynamics studies of lattice resistance in Tantalum, Phys. Rev. B 68 (2003) 014104–014114.
[71] D. R. Trinkle, 2013. URL: http://dtrinkle.matse.illinois.edu.
[72] N. Choly, G. Lu, W.E.,E. Kaxiras, Multiscale simulations in simple metals: a density-functional-based methodology, Phys. Rev. B 71 (2005) 094101–094116.
[73] M. Yu, D.R. Trinkle, R.M. Martin, Energy density in density functional theory: application to crystalline defects and surfaces, Phys. Rev. B 83 (2011) 115113–115122.
[74] N. Lehto, S. Öberg, Effects of dislocation interactions: application to the period-doubled core of the 90° partial in silicon, Phys. Rev. Lett. 80 (1998) 5568–5571.
[75] T. Tsuru, D.C. Chrzan, Effect of solute atoms on dislocation motion in Mg: an electronic structure perspective, Sci. Rep. 5 (2015) 8793–8800.
[76] M.S. Daw, Elasticity effects in electronic structure calculations with periodic boundary conditions, Comput. Mater. Sci. 38 (2006) 293–297.
[77] N. Chaari, E. Clouet, D. Rodney, First-principles study of secondary slip in zirconium, Phys. Rev. Lett. 112 (2014) 075504–075508.
[78] L. Dezerald, D. Rodney, E. Clouet, L. Ventelon, F. Willaime, Plastic anisotropy and dislocation trajectory in BCC metals, Nat. Comm. 6 (2016).
[79] E. Clouet, Dislocation core field. I. Modeling in anisotropic linear elasticity theory, Phys. Rev. B 84 (2011) 224111–224117.
[80] E. Clouet, L. Ventelon, F. Willaime, Dislocation core field. II. Screw dislocation in iron, Phys. Rev. B 84 (2011) 224107–224118.
[81] L. Romaner, C. Ambrosch-Draxl, R. Pippan, Effect of rhenium on the dislocation core structure in tungsten, Phys. Rev. Lett. 104 (2010) 195503–195506.
[82] L. Dezerald, L. Ventelon, E. Clouet, C. Denoual, D. Rodney, F. Willaime, Ab initio modeling of the two-dimensional energy landscape of screw dislocations in bcc transition metals, Phys. Rev. B 89 (2014) 024104–024116.
[83] L. Pizzagalli, P. Beauchamp, H. Jónsson, Calculations of dislocation mobility using nudged elastic band method and first principles DFT calculations,

Philos. Mag. 88 (2008) 91–100.
[84] E. Clouet, Screw dislocation in zirconium: an ab initio study, Phys. Rev. B 86 (2012) 144104–144114.
[85] M. Itakura, H. Kaburaki, M. Yamaguchi, First-principles study on the mobility of screw dislocations in bcc iron, Acta Mater. 60 (2012) 3698–3710.
[86] L. Ventelon, F. Willaime, E. Clouet, D. Rodney, Ab initio investigation of the Peierls potential of screw dislocations in bcc Fe and W, Acta Mater. 61 (2013) 3973–3985.
[87] R. Gröger, V. Vitek, Determination of positions and curved transition pathways of screw dislocations in BCC crystals from atomic displacements, Mater. Sci. Eng. A 643 (2015) 203–210.
[88] C.R. Weinberger, G.J. Tucker, S.M. Foiles, Peierls potential of screw dislocations in bcc transition metals: predictions from density functional theory, Phys. Rev. B 87 (2013) 054114–054121.
[89] J.A. Yasi, T. Nogaret, D.R. Trinkle, Y. Qi, L.G. Hector Jr., W.A. Curtin, Basal and prism dislocation cores in magnesium: comparison of first-principles and embedded-atom-potential methods predictions, Model. Simul. Mater. Sci. Eng. 17 (2009), 055012–052024.
[90] J.A. Yasi, Strength and Ductility of Mg Alloys from First-principles, Ph.D. thesis, Univ. Illinois, Urbana-Champaign, USA, 2013.
[91] J.A. Yasi, L.G. Hector Jr., D.R. Trinkle, Prediction of thermal cross-slip stress in magnesium alloys from direct first-principles data, Acta Mater. 59 (2011) 5652–5660.
[92] J.P. Perdew, K. Burke, M. Ernzerhof, Generalized gradient approximation made simple, Phys. Rev. Lett. 77 (1996) 3865–3868.
[93] D.E. Laughlin, K. Honno (Eds.), Physical Metallurgy, fifth ed., Elsevier, 2015.
[94] D.J. Bacon, Y. Osetsky, D. Rodney, Dislocation–obstacle interactions at the atomic level, in: Dislocations in Solids, vol. 15, Elsevier, 2009, pp. 1–90.
[95] T. Rasmussen, K.W. Jacobsen, T. Leffers, O.B. Pedersen, S.G. Srinivasan, H. Jonsson, Atomistic determination of cross-slip pathway and energetics, Phys. Rev. Lett. 79 (1997), 3676–3079.
[96] S. Aubry, K. Kang, S. Ryu, W. Cai, Energy barrier for homogeneous dislocation nucleation: comparing atomistic and continuum models, Scr. Mat. 64 (2011) 1043–1046.
[97] H. Van Swygenhoven, P.M. Derlet, A.G. Froseth, Nucleation and propagation of dislocations in nanocrystalline fcc metals, Acta Mater. 54 (2006) 1975–1983.
[98] H. Häkkinen, S. Mäkinen, M. Manninen, Edge dislocations in fcc metals: microscopic calculations of core structure and positron states in Al and Cu, Phys. Rev. B 41 (1990) 12441–12453.
[99] J.A. Zimmerman, H. Gao, F.F. Abraham, Generalized stacking fault energies for embedded atom FCC metals, Model. Simul. Mater. Sci. Eng. 8 (2000) 103–115.
[100] A. Hunter, R.F. Zhang, I.J. Beyerlein, The core structure of dislocations and their relationship to the material γ-surface, J. Appl. Phys. 115 (2014) 134314–134318.
[101] C. Brandl, P.M. Derlet, H. Van Swygenhoven, General-stacking-fault energies in highly strained metallic environments: ab initio calculations, Phys. Rev. B 76 (2007).
[102] S. Kibey, J.B. Liu, D.D. Johnson, H. Sehitoglu, Predicting twinning stress in fcc metals: linking twin-energy pathways to twin nucleation, Acta Mater. 55 (2007) 6843–6851.
[103] M. Jahnátek, J. Hafner, M. Krajcí, Shear deformation, ideal strength, and stacking fault formation of fcc metals: a density-functional study of Al and Cu, Phys. Rev. B 79 (2009) 224103–224119.
[104] X.Z. Wu, R. Wang, S.F. Wang, Q.Y. Wei, Ab initio calculations of generalized-stacking-fault energy surfaces and surface energies for FCC metals, App. Surf. Sci. 256 (2010) 6345–6349.
[105] Z.H. Jin, S.T. Dunham, H. Gleiter, H. Hahn, P. Gumbsch, A universal scaling of planar fault energy barriers in face-centered cubic metals, Scr. Mater. 64 (2011) 605–608.
[106] M. Muzyk, Z. Pakiela, K.J. Kurzydlowski, Ab initio calculations of the generalized stacking fault energy in aluminium alloys, Scr. Mater. 64 (2011) 916–918.
[107] R. Wang, S. Wang, X. Wu, Edge dislocation core structures in FCC metals determined from ab initio calculations combined with the improved Peierls-Nabarro equation, Phys. Scr. 83 (2011) 045604–045610.
[108] S.L. Shang, W.Y. Wang, Y. Wang, Y. Du, J.X. Zhang, A.D. Patel, Z.K. Liu, Temperature-dependent ideal strength and stacking fault energy of fcc Ni: a first-principles study of shear deformation, J. Phys. Condens. Matter 24 (2012) 155402–155411.
[109] G. Lu, N. Kioussis, V.V. Bulatov, E. Kaxiras, Generalized-stacking-fault energy surface and dislocation properties of aluminum, Phys. Rev. B 62 (2000) 3099–3108.
[110] G. Lu, N. Kioussis, V.V. Bulatov, E. Kaxiras, Dislocation core properties of aluminum: a first-principles study, Mater. Sci. Eng. A 309 (2001) 142–147.
[111] G. Lu, E. Kaxiras, Can vacancies lubricate dislocation motion in aluminum? Phys. Rev. Lett. 89 (2002) 105501–105504.
[112] G. Schoeck, The core structure of dislocations in Al: a critical assessment, Mater. Sci. Eng. A 333 (2002) 390–396.
[113] C. Shen, Y. Wang, Incorporation of γ-surface to phase field model of dislocations: simulating dislocation dissociation in fcc crystals, Acta Mater. 52 (2004) 683–691.
[114] W. Hollerbauer, H.P. Karnthaler, Beitr. Elektronenmikrosk. Direktabb. Oberfl 14 (1981) 361.
[115] M.J. Mills, M.S. Daw, S.M. Foiles, High-resolution transmission electron microscopy studies of dislocation cores in metals and intermetallic compounds, Ultramicroscopy 56 (1994) 79–93.
[116] P. Hazzledine, H. Karnthaler, E. Wintner, Non-parallel dissociation of dislocations in thin foils, Philos. Mag. 32 (1975) 81–97.
[117] A. Hunter, R.F. Zhang, I.J. Beyerlein, T.C. Germann, M. Koslowski, Dependence of equilibrium stacking fault width in fcc metals on the γ-surface, Model. Simul. Mater. Sci. Eng. 21 (2013) 025015–025033.
[118] I. Shin, A. Ramasubramaniam, C. Huang, L. Hung, E.A. Carter, Orbital-free density functional theory simulations of dislocations in aluminum, Philos. Mag. 89 (2009) 3195–3213.
[119] I. Shin, E.A. Carter, Possible origin of the discrepancy in Peierls stresses of fcc metals: first-principles simulations of dislocation mobility in aluminum, Phys. Rev. B 88 (2013) 064106–064115.
[120] M. Iyer, B. Radhakrishnan, V. Gavini, Electronic-structure study of an edge dislocation in Aluminum and the role of macroscopic deformations on its energetics, J. Mech. Phys. Sol. 76 (2015) 260–275.
[121] S.G. Srinivasan, X.Z. Liao, M.I. Baskes, R.J. McCabe, Y.H. Zhao, Y.T. Zhu, Compact and dissociated dislocations in aluminum: implications for deformation, Phys. Rev. Lett. 94 (2005) 125502–125505.
[122] D. Caillard, Kinetics of dislocations in pure Fe. Part I. In situ straining experiments at room temperature, Acta Mater. 58 (2010) 3493–3503.
[123] J.W. Christian, Some surprising features of the plastic-deformation of body-centered cubic metals and alloys, Metall. Trans. A 14 (1983) 1237–1256.
[124] S.L. Frederiksen, K.W. Jacobsen, Density functional theory studies of screw dislocation core structures in bcc metals, Philos. Mag. 83 (2003) 365–375.
[125] C. Domain, G. Monnet, Simulation of screw dislocation motion in iron by molecular dynamics simulations, Phys. Rev. Lett. 95 (2005) 215506–215509.
[126] D.R. Trinkle, C. Woodward, The chemistry of deformation: how solutes soften pure metals, Science 310 (2005) 1665–1667.
[127] F. Shimizu, S. Ogata, H. Kimizuka, T. Kano, J. Li, H. Kaburaki, First-principles calculation on screw dislocation core properties in bcc molybdenum, J. Earth Simulator 7 (2007) 17–21.
[128] G. Wang, A. Strachan, T. Çağin, W.A. Goddard III, Role of core polarization curvature of screw dislocations in determining the Peierls stress in bcc Ta: a criterion for designing high-performance materials, Phys. Rev. B 67 (2003), 140101(R).
[129] A. Seeger, C. Wüthrich, Nuovo Cim. 33B (1976) 38.
[130] L. Ventelon, F. Willaime, Generalized stacking-faults and screw-dislocation core-structure in bcc iron: a comparison between ab initio calculations and empirical potentials, Philos. Mag. 90 (2010) 1063–1074.
[131] L. Ventelon, F. Willaime, Core structure and Peierls potential of screw dislocations in α-Fe from first principles: cluster versus dipole approaches, Sci. Model. Simul. 14 (2007) 85–94.
[132] L.H. Yang, P. Söderlind, J.A. Moriarty, Accurate atomistic simulation of (a/2)⟨111⟩ screw dislocations and other defects in bcc tantalum, Philos. Mag. A 81 (2001) 1355–1385.
[133] J.-A. Yan, C.-Y. Wang, S.-Y. Wang, Generalized-stacking-fault energy and dislocation properties in bcc Fe: a first-principles study, Phys. Rev. B 70 (2004) 174105–174109.
[134] P.-M. Anglade, G. Jomard, G. Robert, G. Zérah, Computation of the Peierls stress in tantalum with an extended-range modified embedded atom method potential, J. Phys. Condens. Matter (2005) 2003–2018.
[135] C. Denoual, Modeling dislocation by coupling Peierls-Nabarro and element-free Galerkin methods, Comput. Methods Appl. Mech. Eng. 196 (2007) 1915–1923.
[136] L. Dezerald, L. Proville, L. Ventelon, F. Willaime, D. Rodney, First-principles prediction of kink-pair activation enthalpy on screw dislocations in bcc transition metals: V, Nb, Ta, Mo, W, and Fe, Phys. Rev. B 91 (2015) 094105–094111.
[137] H. Li, S. Wurster, C. Motz, L. Romaner, C. Ambrosch-Draxl, R. Pippan, Dislocation-core symmetry and slip planes in tungsten alloys: ab initio calculations and microcantilever bending experiments, Acta Mater. 60 (2012) 748–758.
[138] K. Odbadrakh, A. Rusanu, G.M. Stocks, G.D. Samolyuk, M. Eisenbach, Y. Wang, D.M. Nicholson, Calculated electronic and magnetic structure of screw dislocations in alpha iron, J. Appl. Phys. 109 (2011), 071599–07E161.
[139] Y. Zhao, G. Lu, QM/MM study of dislocation-hydrogen/helium interactions in α-Fe, Model. Simul. Mater. Sci. Eng. 19 (2011) 065004–065016.
[140] G.D. Samolyuk, Y.N. Osetsky, R.E. Stoller, The influence of transition metal solutes on the dislocation core structure and values of the Peierls stress and barrier in tungsten, J. Phys. Condens. Matter 25 (2013) 025403–025411.
[141] J.P. Perdew, Y. Wang, Accurate and simple analytic representation of the electron-gas correlation energy, Phys. Rev. B 45 (1992) 13244–13249.
[142] M. Mendelev, S. Han, D. Srolovitz, G. Ackland, D. Sun, M. Asta, Development of new interatomic potentials appropriate for crystalline and liquid iron, Philos. Mag. 83 (2003) 3977–3994.
[143] P.A. Gordon, T. Neeraj, M.I. Mendelev, Screw dislocation mobility in BCC Metals: a refined potential description for α-Fe, Philos. Mag. 91 (2011) 3931–3945.
[144] M. Mrovec, D. Nguyen-Manh, C. Elsässer, P. Gumbsch, Magnetic bond-order potential for iron, Phys. Rev. Lett. 106 (2011) 246402–246405.
[145] M. Mrovec, D. Nguyen-Manh, D.G. Pettifor, V. Vitek, Bond-order potential for molybdenum: application to dislocation behavior, Phys. Rev. B 69 (2004) 094115–094130.

[146] M. Mrovec, R. Gröger, A.G. Bailey, D. Nguyen-Manh, C. Elsässer, V. Vitek, Bond-order potential for simulations of extended defects in tungsten, Phys. Rev. B 75 (2007) 104119–104134.
[147] D. Rodney, L. Proville, Stress-dependent Peierls potential: influence on kink-pair activation, Phys. Rev. B 79 (2009) 094108–094116.
[148] R. Gröger, V. Vitek, Stress dependence of the Peierls barrier of 1/2⟨111⟩ screw dislocations in bcc metals, Acta Mater. 61 (2013) 6362–6371.
[149] R. Gröger, V. Vitek, Explanation of the discrepancy between the measured and atomistically calculated yield stresses in body-centred cubic metals, Philos. Mag. Lett. 87 (2007) 113–120.
[150] V.V. Bulatov, W. Cai, Nodal effects in dislocation mobility, Phys. Rev. Lett. 89 (2002) 115501–115504.
[151] L. Proville, D. Rodney, M.-C. Marinica, Quantum effect on thermally activated glide of dislocations, Nat. Mater. 11 (2012) 845–849.
[152] B. Barvinschi, L. Proville, D. Rodney, Quantum Peierls stress of straight and kinked dislocations and effect of non-glide stresses, Model. Simul. Mater. Sci. Eng. 22 (2014) 025006–025019.
[153] Z.M. Chen, M. Mrovec, P. Gumbsch, Atomistic aspects of screw dislocation behavior in α-iron and the derivation of microscopic yield criterion, Model. Simul. Mater. Sci. Eng. 21 (2013) 055023–055040.
[154] R. Gröger, Which stresses affect the glide of screw dislocations in bcc metals? Philos. Mag. 94 (2014) 2021–2030.
[155] L. Ventelon, F. Willaime, P. Leyronnas, Atomistic simulation of single kinks of screw dislocations in α-Fe, J. Nucl. Mater. 386–388 (2009) 26–29.
[156] L. Proville, L. Ventelon, D. Rodney, Prediction of the kink-pair formation enthalpy on screw dislocations in α-iron by a line tension model parametrized on empirical potentials and first-principles calculations, Phys. Rev. B 87 (2013) 144106–144113.
[157] G.I. Taylor, The deformation of crystals of β-brass, Proc. Roy. Soc. Lond. A 118 (1928) 1–24.
[158] K. Edagawa, T. Suzuki, S. Takeuchi, Motion of a screw dislocation in a two-dimensional Peierls potential, Phys. Rev. B 55 (1997) 6180–6187.
[159] K. Edagawa, T. Suzuki, S. Takeuchi, Plastic anisotropy in b.c.c. transition metals, Mater. Sci. Eng. A 234–236 (1997) 1103–1105.
[160] N.I. Medvedeva, Y.N. Gornostyrev, A.J. Freeman, Solid solution softening and hardening in the group-V and group-VI bcc transition metals alloys: first principles calculations and atomistic modeling, Phys. Rev. B 76 (2007) 212104–212107.
[161] L. Romaner, V. Razumovskiy, R. Pippan, Core polarity of screw dislocations in Fe-Co alloys, Philos. Mag. Lett. 94 (2014) 334–341.
[162] M. Itakura, H. Kaburaki, M. Yamaguchi, T. Okita, The effect of hydrogen atoms on the screw dislocation mobility in bcc iron: a first-principles study, Acta Mater. 61 (2013) 6857–6867.
[163] D. Terentyev, V. Dubinko, A. Bakaev, Y. Zayachuk, W.V. Renterghem, P. Grigorev, Dislocations mediate hydrogen retention in tungsten, Nucl. Fusion 54 (2014) 042004–042008.
[164] L. Ventelon, B. Lüthi, E. Clouet, L. Proville, B. Legrand, D. Rodney, F. Willaime, Dislocation core reconstruction induced by carbon segregation in bcc iron, Phys. Rev. B 91 (2015) 220102–220106.
[165] Y. Hanlumyuang, P.A. Gordon, T. Neeraj, D.C. Chrzan, Interactions between carbon solutes and dislocations in bcc iron, Acta Mater. 58 (2010) 5481–5490.
[166] B. Legrand, Relations entre la structure électronique et la facilité de glissement dans les métaux hexagonaux compacts, Philos. Mag. B 49 (1984) 171–184.
[167] P. Villars, L.D. Calvert, Pearson's Handbook of Crystallographic Data for Intermetallic Phases, American Society for Metals, Materials Park, OH, USA, 1985.
[168] R. Bechmann, R.F.S. Hearmon, Elastic, piezoelectric, piezooptic, and electro-optic constants of crystals, in: K.-H. Hellwege, A.M. Hellwege (Eds.), Landolt-börnstein, Group III, vol. 1, Springer, Berlin, 1966.
[169] L. Wen, P. Chen, Z.-F. Tong, B.-Y. Tang, L.-M. Peng, W.-J. Ding, A systematic investigation of stacking faults in magnesium via first-principles calculation, Eur. Phys. J. B 72 (2009) 397–403.
[170] Z. Pei, L.-F. Zhu, M. Friák, S. Sandlöbes, J. von Pezold, H.W. Sheng, C.P. Race, S. Zaefferer, B. Svendsen, D. Raabe, J. Neugebauer, Ab initio and atomistic study of generalized stacking fault energies in Mg and Mg–Y alloys, New J. Phys. 15 (2013) 043020–043038.
[171] J. Zhang, Y. Dou, H. Dong, Intrinsic ductility of Mg-based binary alloys: a first-principles study, Scr. Mater. 89 (2014) 13–16.
[172] Y. Dou, J. Zhang, Effects of structural relaxation on the generalized stacking fault energies of hexagonal-close-packed system from first-principles calculations, Comp. Mater. Sci. 98 (2015) 405–409.
[173] E.S. Fisher, C.J. Renken, Single-crystal moduli and the hcp → bcc transformation in Ti, Zr and Hf, Phys. Rev. 135 (1964) A482–A494.
[174] C. Domain, Simulations atomiques ab initio des effets de l'hydrogène et de l'iode dans le zirconium, Ph.D. thesis, Univ. Lille 1, France, 2002.
[175] C. Domain, Ab initio modelling of defect properties with substitutional and interstitials elements in steels and Zr alloys, J. Nucl. Mater. 351 (2006) 1–19.
[176] A. Poty, J.-M. Raulot, H. Xu, J. Bai, C. Schuman, J.-S. Lecomte, M.-J. Philippe, C. Esling, Classification of the critical resolved shear stress in the hexagonal-close-packed materials by atomic simulation: application to α-zirconium and α-titanium, J. Appl. Phys. 110 (2011) 014905–014919.
[177] M. Ghazisaeidi, D.R. Trinkle, Core structure of a screw dislocation in Ti from density functional theory and classical potentials, Acta Mater. 60 (2012) 1287–1292.
[178] M. Ghazisaeidi, D.R. Trinkle, Interaction of oxygen interstitials with lattice faults in Ti, Acta Mater. 76 (2014) 82–86.
[179] P. Kwasniak, H. Garbacz, K.J. Kurzydlowski, Solid solution strengthening of hexagonal titanium alloys: restoring forces and stacking faults calculated from first principles, Acta Mater. 102 (2016) 304–314.
[180] E. Clouet, D. Caillard, N. Chaari, F. Onimus, D. Rodney, Dislocation locking versus easy glide in titanium and zirconium, Nat. Mater. 14 (2015) 931–936.
[181] L. Liang, Simulation ab initio des défauts étendus du Ti α en présence d'interstitiels H et O, Ph.D. thesis, Univ. Paris Saclay, France, 2016.
[182] C. Domain, R. Besson, A. Legris, Atomic-scale ab-initio study of the Zr–H system: I. Bulk properties, Acta Mater. 50 (2002) 3513–3526.
[183] C. Domain, R. Besson, A. Legris, Atomic-scale ab initio study of the Zr–H system: II. Interaction of H with plane defects and mechanical properties, Acta Mater. 52 (2004) 1495–1502.
[184] Y. Udagawa, M. Yamaguchi, H. Abe, N. Sekimura, T. Fuketa, Ab initio study on plane defects in zirconium-hydrogen solid solution and zirconium hydride, Acta Mater. 58 (2010) 3927–3938.
[185] D. Vanderbilt, Soft self-consistent pseudopotentials in a generalized eigenvalue formalism, Phys. Rev. B 41 (1990) 7892–7895.
[186] D. Bacon, V. Vitek, Atomic-scale modeling of dislocations and related properties in the hexagonal-close-packed metals, Metall. Mater. Trans. A 33 (2002) 721–733.
[187] P.M. Kelly, H.P. Ren, D. Qiu, M.X. Zhang, Identifying close-packed planes in complex crystal structures, Acta Mater. 58 (2010) 3091–3095.
[188] J. Yasi, L.G. Hector, D.R. Trinkle, Prediction of thermal cross-slip stress in magnesium alloys from a geometric interaction model, Acta Mater. 60 (2012) 2350–2358.
[189] C. Wang, H.-Y. Wang, H.-Y. Zhang, X.-L. Nan, E.-S. Xue, Q.-C. Jiang, First-principles study of generalized-stacking-fault (GSF) energy in Mg with Al and Zn alloyings, J. Alloys Compd. 575 (2013) 423–433.
[190] A. De Crecy, A. Bourret, S. Naka, A. Lasalmonie, High resolution determination of the core structure of 1/3⟨11$\bar{2}$0⟩{10$\bar{1}$} edge dislocation in titanium, Philos. Mag. A 47 (1983) 245–254.
[191] L.J. Teutonico, Dislocations in hexagonal crystals, Mater. Sci. Eng. 6 (1970) 27–47.
[192] T. Uesugi, M. Kohyama, M. Kohzu, K. Higashi, Generalized stacking fault energy and dislocation properties for various slip systems in magnesium: a first-principles study, Mater. Sci. Forum 419–422 (2003) 225–230.
[193] A.E. Smith, Surface, interface and stacking fault energies of magnesium from first principles calculations, Surf. Sci. 601 (2007) 5762–5765.
[194] A. Datta, U.V. Waghmare, U. Ramamurty, Structure and stacking faults in layered Mg–Zn–Y alloys: a first-principles study, Acta Mater. 56 (2008) 2531–2539.
[195] I. Shin, E.A. Carter, Orbital-free density functional theory simulations of dislocations in magnesium, Model. Simul. Mater. Sci. Eng. 20 (2012) 015006–015028.
[196] T. Tsuru, Y. Udagawa, M. Yamaguchi, M. Itakura, H. Kaburaki, Y. Kaji, Solution softening in magnesium alloys: the effect of solid solutions on the dislocation core structure and nonbasal slip, J. Phys. Condens. Matter 25 (2013) 022202–022206.
[197] N. Chaari, E. Clouet, D. Rodney, First order pyramidal slip of 1/3⟨1$\bar{2}$10⟩ screw dislocations in zirconium, Metall. Mater. Trans. A 45 (2014) 5898–5905.
[198] A. Serra, R.C. Pond, D.J. Bacon, Computer simulation of the structure and mobility of twinning dislocations in h.c.p. metals, Acta Metall. Mater. 39 (1991) 1469–1480.
[199] N. Tarrat, M. Benoit, J. Morillo, Core structure of screw dislocations in hcp Ti: an ab initio DFT study, Int. J. Mater. Res. 100 (2009) 329–332.
[200] N. Tarrat, M. Benoit, D. Caillard, L. Ventelon, N. Combe, J. Morillo, Screw dislocation in hcp Ti: DFT dislocation excess energies and metastable core structures, Model. Simul. Mater. Sci. Eng. 22 (2014) 055016–055034.
[201] Q. Yu, L. Qi, T. Tsuru, R. Traylor, D. Rugg, J.W. Morris, M. Asta, D.C. Chrzan, A.M. Minor, Origin of dramatic oxygen solute strengthening effect in titanium, Science 347 (2015) 635–639.
[202] K.E.J. Rapperport, C.S. Hartley, Deformation modes of zirconium at 77, 575, and 1075 K, Trans. AIME 218 (1960) 869–876.
[203] D. Mills, G.B. Craig, The plastic deformation of zirconium-oxygen alloy single crystals in the range 77 to 950 K, Trans. AIME 242 (1968) 1881–1890.
[204] P. Soo, G.T. Higgins, The deformation of zirconium-oxygen single crystals, Acta Metall. 16 (1968) 177–186.
[205] A. Akhtar, A. Teghtsoonian, Plastic deformation of zirconium single crystals, Acta Metall. 19 (1971) 655–663.
[206] S. Farenc, D. Caillard, A. Couret, An in situ study of prismatic glide in α titanium at low temperatures, Acta Metall. Mater. 41 (1993) 2701–2709.
[207] S. Farenc, D. Caillard, A. Couret, A new model for the peak of activation area of α titanium, Acta Metall. Mater. 43 (1995) 3669–3678.
[208] H. Conrad, Effect of interstitial solutes on the strength and ductility of titanium, Prog. Mater. Sci. 26 (1981) 123–403.
[209] D. Caillard, J.L. Martin, Thermally Activated Mechanisms in Crystal Plasticity, Pergamon Materials Series, Pergamon, 2003.
[210] D. Banerjee, J.C. Williams, Perspectives on titanium science and technology, Acta Mater. 61 (2013) 844–879.
[211] S. Naka, A. Lasalmonie, P. Costa, L.P. Kubin, The low-temperature plastic deformation of α titanium and the core structure of *a*-type screw dislocations, Philos. Mag. A 57 (1988) 717–740.

[212] N. Chaari, Modélisation ab initio de la plasticité dans les métaux hexagonaux purs, zirconium et titane, et effet de l'oxygène, Ph.D. thesis, Univ. Grenoble Alpes, 2015.
[213] M. Itakura, H. Kaburaki, M. Yamaguchi, T. Tsuru, Atomistic study on the cross-slip process of a screw⟨a⟩ dislocation in magnesium, Model. Simul. Mater. Sci. Eng. 23 (2015) 065002–065020.
[214] A. Couret, D. Caillard, W. Püschl, G. Schoeck, Prismatic glide in divalent h.c.p, Met. Philos. Mag. A 63 (1991) 1045–1057.
[215] J.A. Yasi, L.G. Hector Jr., D.R. Trinkle, First-principles data for solid-solution strengthening of magnesium: from geometry and chemistry to properties, Acta Mater. 58 (2010) 5704–5713.
[216] H. Numakura, Y. Minonishi, M. Koiwa, ⟨$\bar{1}$1$\bar{2}$3⟩{1011} slip in zirconium, Philos. Mag. A 63 (1991) 1077–1084.
[217] I.P. Jones, W.B. Hutchinson, Stress-state dependence of slip in titanium–6Al–4V and other h.c.p. metals, Acta Metall. 29 (1981) 951–968.
[218] H. Numakura, Y. Minonishi, M. Koiwa, ⟨$\bar{1}$1$\bar{2}$3⟩{1011} slip in titanium polycrystals at room temperature, Scr. Metall. 20 (1986) 1581–1586.
[219] Y. Minonishi, S. Morozumi, H. Yoshinaga, {11$\bar{2}$2}⟨$\bar{1}$1$\bar{2}$3⟩ slip in titanium, Scr. Metall. 16 (1982) 427–430.
[220] S. Sandlöbes, M. Friák, J. Neugebauer, D. Raabe, Basal and non-basal dislocation slip in Mg–Y, Mater. Sci. Eng. A 576 (2013) 61–68.
[221] H. Fan, J.A. El-Awady, Towards resolving the anonymity of pyramidal slip in magnesium, Mater. Sci. Eng. A 644 (2015) 318–324.
[222] J. Geng, M.F. Chisholm, R.K. Mishra, K.S. Kumar, An electron microscopy study of dislocation structures in Mg single crystals compressed along [0001] at room temperature, Philos. Mag. 95 (2015) 3910–3932.
[223] K.Y. Xie, Z. Alam, A. Caffee, K.J. Hemker, Pyramidal I slip in c-axis compressed Mg single crystals, Scr. Mater. 112 (2016) 75–78.
[224] T. Nogaret, W.A. Curtin, J.A. Yasi, L.G. Hector Jr., D.R. Trinkle, Atomistic study of edge and screw ⟨c+a⟩ dislocations in magnesium, Acta Mater. 58 (2010) 4332–4343.
[225] E. Clouet, unpublished (2016).
[226] W. Szewc, L. Pizzagalli, S. Brochard, E. Clouet, Onset of plasticity in zirconium in relation with hydrides precipitation, Acta Mater. 114 (2016) 126–135.
[227] B. Li, P.F. Yan, M.L. Sui, E. Ma, Transmission electron microscopy study of stacking faults and their interaction with pyramidal dislocations in deformed Mg, Acta Mater. 58 (2010) 173–179.
[228] J.R. Morris, J. Scharff, K.M. Ho, D.E. Turner, Y.Y. Ye, M.H. Yoo, Prediction of a {1122} hcp stacking fault using a modified generalized stacking-fault calculation, Philos. Mag. A 76 (1997) 1065–1077.
[229] C. Wang, H.-Y. Zhang, H.-Y. Wang, G.-J. Liu, Q.-C. Jiang, Effects of doping atoms on the generalized stacking-fault energies of Mg alloys from first-principles calculations, Scr. Mater. 69 (2013) 445–448.
[230] J.-F. Stohr, J.-P. Poirier, Etude en microscopie électronique du glissement pyramidal {11$\bar{2}$2}⟨11$\bar{2}$3⟩ dans le magnésium, Philos. Mag. 25 (1972) 1313–1329.
[231] J. Geng, M.F. Chisholm, R.K. Mishra, K.S. Kumar, The structure of ⟨c+a⟩ type dislocation loops in magnesium, Philos. Mag. Lett. 94 (2014) 1–10.
[232] S. Sandlöbes, M. Friák, S. Zaefferer, A. Dick, S. Yi, D. Letzig, Z. Pei, L.-F. Zhu, J. Neugebauer, D. Raabe, The relation between ductility and stacking fault energies in Mg and Mg–Y alloys, Acta Mater. 60 (2012) 3011–3021.
[233] S.R. Agnew, L. Capolungo, C.A. Calhoun, Connections between the basal I1 "growth" fault and ⟨c+a⟩ dislocations, Acta Mater. 82 (2015) 255–265.
[234] M. Ghazisaeidi, L.G. Hector, W.A. Curtin, First-principles core structures of edge and screw ⟨c+a⟩ dislocations in Mg, Scr. Mater. 75 (2014) 42–45.
[235] M. Itakura, H. Kaburaki, M. Yamaguchi, T. Tsuru, Novel cross-slip mechanism of pyramidal screw dislocations in magnesium, Phys. Rev. Lett. 116 (2016) 225501.
[236] Z. Wu, W.A. Curtin, The origins of high hardening and low ductility in magnesium, Nature 526 (2015) 62–67.
[237] R. Jones, A. Umerski, P. Sitch, M.I. Heggie, S. Öberg, First-principles calculations of dislocations in semiconductors, Phys. Stat. Sol.(a) 137 (1993) 389–399.
[238] O. Ueda, S. Pearton (Eds.), Materials and Reliability Handbook for Semiconductor Optical and Electron Devices, Springer-Verlag, New York, 2013.
[239] C.R. Miranda, R.W. Nunes, A. Antonelli, Temperature effects on dislocation core energies in silicon and germanium, Phys. Rev. B 67 (2003) 235201–235208.
[240] J. Rabier, L. Pizzagalli, J.-L. Demenet, Dislocations in silicon at high stress, in: L. Kubin, J.P. Hirth (Eds.), Dislocation in Solids, vol. 16, Elsevier, 2010, p. 47.
[241] E. Kaxiras, M.S. Duesbery, Free energies of generalized stacking faults in Si and implications for the brittle-ductile transition, Phys. Rev. Lett. 70 (1993) 3752–3755.
[242] P. Käckell, J. Furthmüller, F. Bechstedt, Stacking faults in group-IV crystals: an *ab initio* study, Phys. Rev. B 58 (1998) 1326–1330.
[243] J. Spence, Experimental studies of dislocation core defects, in: F.R.N. Nabarro, J.P. Hirth (Eds.), Dislocations in Solids, vol. 13, Elsevier, 2007, p. 421.
[244] J. Bennetto, R.W. Nunes, D. Vanderbilt, Period-doubled structure for the 90° partial dislocation in silicon, Phys. Rev. Lett. 79 (1997) 245–248.
[245] R.W. Nunes, D. Vanderbilt, Models of core reconstruction for the 90° partial dislocation in semiconductors, J. Phys. Condens. Matter 12 (2000) 10021–10027.
[246] X. Blase, K. Lin, A. Canning, S.G. Louie, D.C. Chrzan, Structure and energy of the 90° partial dislocation in diamond: A combined ab initio and elasticity theory analysis, Phys. Rev. Lett. 84 (2000) 5780–5783.
[247] S.P. Beckman, D.C. Chrzan, Reconstruction energies of partial dislocations in cubic semiconductors, Phys. Rev. B 76 (2007), 144110–144014.
[248] S.P. Beckman, X. Xu, P. Specht, E.R. Weber, C. Kisielowski, D.C. Chrzan, Ab initio prediction of the structure of glide set dislocation cores in GaAs, J. Phys. Condens. Matter 14 (2002) 12673–12680.
[249] J.F. Justo, V.V. Bulatov, S. Yip, Dislocation core reconstruction and its effect on dislocation mobility in silicon, J. Appl. Phys. 86 (1999) 4249–4257.
[250] M.S. Duesbery, G.Y. Richardson, The dislocation core in crystalline materials, Crit. Rev. Solid State Mater. Sci. 17 (1991) 1–46.
[251] A. Valladares, A.K. Petford-Long, A.P. Sutton, The core reconstruction of the 90° partial dislocation in silicon, Philos. Mag. Lett. 79 (1999) 9–17.
[252] M. Heggie, R. Jones, Solitons and the electrical and mobility properties of dislocations in silicon, Philos. Mag. B 48 (1983) 365–377.
[253] G. Csányi, S. Ismail-Beigi, T.A. Arias, Paramagnetic structure of the soliton of the 30° partial dislocation in silicon, Phys. Rev. Lett. 80 (1998) 3984–3987.
[254] A. Valladares, A.P. Sutton, First principles simulations of antiphase defects on the SP 90° partial dislocation in silicon, J. Phys. Condens. Matter 18 (2006) 3735–3744.
[255] N. Lehto, M.I. Heggie, Modelling of dislocations in c-Si, in: R. Hull (Ed.), Properties of Crystalline Silicon, Number 20 in EMIS Datareviews, INSPEC, London, 1999, p. 357.
[256] R.W. Nunes, J. Bennetto, D. Vanderbilt, Core reconstruction of the 90° partial dislocation in nonpolar semiconductors, Phys. Rev. B 58 (1998) 12563–12566.
[257] C.P. Ewels, N.T. Wilson, M.I. Heggie, R. Jones, P.R. Briddon, Graphitization at diamond dislocation cores, J. Phys. Condens. Matter 13 (2001) 8965–8972.
[258] A.T. Blumenau, M.I. Heggie, C.J. Fall, R. Jones, T. Frauenheim, Dislocations in diamond: core structures and energies, Phys. Rev. B 65 (2002) 205205–205212.
[259] A.T. Blumenau, C.J. Fall, R. Jones, M.I. Heggie, P.R. Briddon, T. Frauenheim, S. Öberg, Straight and kinked 90° partial dislocations in diamond and 3C–SiC, J. Phys. Condens. Matter 14 (2002) 12741–12747.
[260] J.F. Justo, R.W. Nunes, L.V.C. Assali, Microscopic structure of the 90° and 30° partial dislocations in gallium arsenide, J. Phys. Condens. Matter 14 (2002) 12749–12754.
[261] P.K. Sitch, R. Jones, S. Öberg, M.I. Heggie, Ab initio investigation of the dislocation structure and activation energy for dislocation motion in silicon carbide, Phys. Rev. B 52 (1995) 4951–4955.
[262] A.T. Blumenau, C.J. Fall, R. Jones, S. Öberg, T. Frauenheim, P.R. Briddon, Structure and motion of basal dislocations in silicon carbide, Phys. Rev. B 68 (2003) 174108–174121.
[263] J.F. Justo, A. Fazzio, A. Antonelli, Dislocation core reconstruction in zinc-blende semiconductors, J. Phys. Condens. Matter 12 (2000) 10039–10044.
[264] P. Komninou, J. Kioseoglou, G.P. Dimitrakopulos, T. Kehagias, T. Karakostas, Partial dislocations in wurtzite GaN, Phys. Stat. Sol.(a) 202 (2005) 2888–2899.
[265] G. Savini, A.T. Blumenau, M.I. Heggie, S. Öberg, Structure and energy of partial dislocations in wurtzite–GaN, Phys. Stat. Sol.(c) 4 (2007) 2945–2949.
[266] L. Pizzagalli, J. Godet, J. Guénolé, S. Brochard, Dislocation cores in silicon: new aspects from numerical simulations, J. Phys. Conf. Ser. 281 (2011) 012002–012009.
[267] L. Pizzagalli, P. Beauchamp, J. Rabier, Undissociated screw dislocations in silicon: calculations of core structure and energy, Philos. Mag. A 83 (2003) 1191–1204.
[268] T.A. Arias, J.D. Joannopoulos, Ab initio theory of dislocations: from close-range spontaneous annihilation to the long-range continuum limit, Phys. Rev. Lett. 73 (1994) 680–683.
[269] V. Celli, Screw dislocation in crystals with diamond structure, J. Phys. Chem. Solids 19 (1961) 100–104.
[270] C.-Z. Wang, J. Li, K.-M. Ho, S. Yip, Undissociated screw dislocation in Si: glide or shuffle set? Appl. Phys. Lett. 89 (2006) 051910–051912.
[271] L. Pizzagalli, P. Beauchamp, J. Rabier, Stability of undissociated screw dislocations in zinc-blende covalent materials from first principle simulations, Europhys. Lett. 72 (2005) 410–415.
[272] L. Pizzagalli, Stability and mobility of screw dislocations in 4H, 2H and 3C silicon carbide, Acta Mater. 78 (2014) 236–244.
[273] S. Izumi, H. Ohta, C. Takahashi, T. Suzuki, H. Saka, Shuffle-set dislocation nucleation in semiconductor silicon device, Philos. Mag. Lett. 90 (2010) 707–714.
[274] J. Rabier, A. Montagne, J.L. Demenet, J. Michler, R. Ghisleni, Silicon micropillars: high stress plasticity, Phys. Stat. Sol.(c) 10 (2013) 11–15.
[275] L. Pizzagalli, J. Godet, S. Brochard, Glissile dislocations with transient cores in silicon, Phys. Rev. Lett. 103 (2009) 065505–065508.
[276] A.T. Blumenau, J. Elsner, R. Jones, M.I. Heggie, S. Öberg, T. Frauenheim, P.R. Briddon, Dislocations in hexagonal and cubic GaN, J. Phys. Condens. Matter 12 (2000) 10223–10233.
[277] F. Liu, M. Mostoller, V. Milman, M.F. Chisholm, T. Kaplan, Electronic and elastic properties of edge dislocations in Si, Phys. Rev. B 51 (1995) 17192–17195.
[278] G. Cicero, L. Pizzagalli, A. Catellani, Ab initio study of misfit dislocations at the SiC/Si(001) interface, Phys. Rev. Lett. 89 (2002) 156101–156104.
[279] A. Béré, A. Serra, Atomic structure of dislocation cores in GaN, Phys. Rev. B 65 (2002) 205323–205332.
[280] I. Belabbas, G. Nouet, P. Komninou, Atomic core configurations of the $\vec{a}$-screw basal dislocation in wurtzite GaN, J. Cryst. Growth 300 (2007)

212–216.
[281] I. Belabbas, J. Chen, P. Komninou, G. Nouet, The 60° basal dislocation in wurtzite GaN: Energetics, electronic and core structures, Comp. Mater. Sci. 79 (2013) 118–124.
[282] Z. Liliental-Weber, J. Jasinski, D.N. Zakharov, GaN growth in polar and non-polar directions, Opto-Electron Rev. 12 (2004) 339–346.
[283] M. Matsubara, J. Godet, L. Pizzagalli, E. Bellotti, Properties of threading screw dislocation core in wurtzite GaN studied by Heyd-Scuseria-Ernzerhof hybrid functional, Appl. Phys. Lett. 103 (2013) 262107–262110.
[284] J. Elsner, R. Jones, P.K. Sitch, V.D. Porezag, M. Elstner, T. Frauenheim, M.I. Heggie, S. Öberg, P.R. Briddon, Theory of threading edge and screw dislocations in GaN, Phys. Rev. Lett. 79 (1997) 3672–3675.
[285] J.E. Northrup, Screw dislocations in GaN: the Ga-filled core model, Appl. Phys. Lett. 78 (2001) 2288–2290.
[286] J.E. Northrup, Theory of intrinsic and H-passivated screw dislocations in GaN, Phys. Rev. B 66 (2002) 045204–045208.
[287] I. Belabbas, J. Chen, G. Nouet, A new atomistic model for the threading screw dislocation core in wurtzite GaN, Comput. Mater. Sci. 51 (2011) 206–216.
[288] I. Belabbas, J. Chen, G. Nouet, Electronic structure and metallization effects at threading dislocation cores in GaN, Comp. Mater. Sci. 90 (2014) 71–81.
[289] A.F. Wright, U. Grossner, The effect of doping and growth stoichiometry on the core structure of a threading edge dislocation in GaN, Appl. Phys. Lett. 73 (1998) 2751–2753.
[290] A. Alkauskas, P. Deák, J. Neugebauer, A. Pasquarello, C.G.V. de Walle (Eds.), Advanced Calculations for Defects in Materials, Electronic Structure Methods, Wiley-VCH, Weinheim, Germany, 2011.
[291] L. Lymperakis, J. Neugebauer, M. Albrecht, T. Remmele, H.P. Strunk, Strain induced deep electronic states around threading dislocations in GaN, Phys. Rev. Lett. 93 (2004) 196401–196404.
[292] A.F. Wright, J. Furthmüller, Theoretical investigation of edge dislocations in AlN, Appl. Phys. Lett. 72 (1998) 3467–3469.
[293] E. Kalesaki, J. Kioseoglou, L. Lymperakis, P. Komninou, T. Karakostas, Effect of edge threading dislocations on the electronic structure of InN, Appl. Phys. Lett. 98 (2011) 072103–072105.
[294] M. Heggie, R. Jones, A. Umerski, Interaction of impurities with dislocation cores in silicon, Philos. Mag. A 63 (1991) 571–584.
[295] M.I. Heggie, R. Jones, A. Umerski, Ab initio total energy calculations of impurity pinning in silicon, Phys. Stat. Sol.(a) 138 (1993) 383–387.
[296] A. Maiti, T. Kaplan, M. Mostoller, M.F. Chisholm, S.J. Pennycook, S.T. Pantelides, Ordering of as impurities in a Si dislocation core, Appl. Phys. Lett. 70 (1997) 336–338.
[297] T.M. Schmidt, J.T. Arantes, A. Fazzio, First principles calculations of as impurities in the presence of a 90° partial dislocation in Si, Braz. J. Phys. 36 (2006) 261–263.
[298] A. Antonelli, J.F. Justo, A. Fazzio, Interaction of as impurities with 30° partial dislocations in Si: An ab initio investigation, J. Appl. Phys. 91 (2002) 5892–5895.
[299] T. Kaplan, F. Liu, M. Mostoller, M.F. Chisholm, V. Milman, First-principles study of impurity segregation in edge dislocations in Si, Phys. Rev. B 61 (2000) 1674–1676.
[300] B. Ziebarth, M. Mrovec, C. Elsässer, P. Gumbsch, Interstitial iron impurities at cores of dissociated dislocations in silicon, Phys. Rev. B 92 (2015) 195308–195314.
[301] F. Bernardini, L. Colombo, Interaction of doping impurities with the 30° partial dislocation in SiC: An ab initio investigation, Phys. Rev. B 72 (2005) 085215–085224.
[302] M. Matsubara, J. Godet, L. Pizzagalli, Investigation of the interaction between hydrogen and screw dislocation in silicon by first-principles calculations, J. Phys. Condens. Matter 22 (2010) 035803–035809.
[303] M. Matsubara, J. Godet, L. Pizzagalli, Theoretical study of hydrogen stability and aggregation in dislocation cores in silicon, Phys. Rev. B 82 (2010) 024107–024117.
[304] J.P. Goss, R. Jones, M.I. Heggie, C.P. Ewels, P.R. Briddon, S. Öberg, Theory of hydrogen in diamond, Phys. Rev. B 65 (2002) 115207–115219.
[305] R. Hull, Properties of Crystalline Silicon, Number 20 in EMIS Datareviews, INSPEC, London, 1999.
[306] H. Saka, K. Yamamoto, S. Arai, K. Kuroda, In-situ TEM observation of transformation of dislocations from shuffle to glide sets in Si under supersaturation of interstitials, Philos. Mag. 86 (2006) 4841–4850.
[307] N. Lehto, S. Öberg, Interaction of vacancies with partial dislocations in silicon, Phys. Rev. B 56 (1997) R12706–R12709.
[308] J.F. Justo, M. de Koning, W. Cai, V.V. Bulatov, Vacancy interaction with dislocations in silicon: the shuffle-glide competition, Phys. Rev. Lett. 84 (2000) 2172–2175.
[309] A. Antonelli, J.F. Justo, A. Fazzio, Arsenic segregation, pairing and mobility on the cores of partial dislocations in silicon, J. Phys. Condens. Matter 14 (2002) 12761–12765.
[310] M. Miyata, T. Fujiwara, Ab initio calculation of Peierls stress in silicon, Phys. Rev. B 63 (2001) 045206–045214.
[311] J. Godet, S. Brochard, L. Pizzagalli, P. Beauchamp, J.M. Soler, Dislocation formation from a surface step in semiconductors: an ab initio study, Phys. Rev. B 73 (2006) 092105–092108.
[312] G. Lu, The Peierls-Nabarro model of dislocations: a venerable theory and its current development, in: S. Yip (Ed.), Handbook of Materials Modeling, Methods and Models, 2.20, vol. I, Springer, 2005, p. 1.
[313] Y.-M. Juan, E. Kaxiras, Generalized stacking fault energy surfaces and dislocation properties of silicon: a first-principles theoretical study, Philos. Mag. 74 (1996) 1367–1384.
[314] L. Pizzagalli, A. Pedersen, A. Arnaldsson, H. Jónsson, P. Beauchamp, Theoretical study of kinks on screw dislocation in silicon, Phys. Rev. B 77 (2008) 064106–064119.
[315] V.V. Bulatov, S. Yip, A.S. Argon, Atomic modes of dislocation mobility in silicon, Philos. Mag. A 72 (1995) 453–496.
[316] R.W. Nunes, J. Benetto, D. Vanderbilt, Atomic structure of dislocation kinks in silicon, Phys. Rev. B 57 (1998) 10388–10397.
[317] Y.M. Huang, J.C.H. Spence, O.F. Sankey, Dislocation kink motion in silicon, Phys. Rev. Lett. 74 (1995) 3392–3395.
[318] S. Öberg, P.K. Sitch, R. Jones, M.I. Heggie, First-principles calculations of the energy barrier to dislocation motion in Si and GaAs, Phys. Rev. B 51 (1995) 13138–13145.
[319] A. Valladares, A.P. Sutton, First principles simulations of kink defects on the SP 90° partial dislocation in silicon, Prog. Mater. Sci. 52 (2007) 421–463.
[320] A. Valladares, J.A. White, A.P. Sutton, First principles simulations of the structure, formation, and migration energies of kinks on the 90° partial dislocation in silicon, Phys. Rev. Lett. 81 (1998) 4903–4906.
[321] V.V. Bulatov, Bottomless complexity of core structure and kink mechanisms of dislocation motion in silicon, Scr. Mater. 45 (2001) 1247–1252.
[322] A. Pedersen, L. Pizzagalli, H. Jónsson, Finding mechanism of transitions in complex systems: formation and migration of dislocation kinks in a silicon crystal, J. Phys. Condens. Matter 21 (2009) 084210–084217.
[323] I. Yonenaga, Dislocation-impurity interaction in Si, Mater. Sci. Eng. B 124-125 (2005) 293–296.
[324] C.P. Ewels, S. Leoni, M.I. Heggie, P. Jemmer, E. Hernández, R. Jones, P.R. Briddon, Hydrogen interaction with dislocations in Si, Phys. Rev. Lett. 84 (2000) 690–693.
[325] M.I. Heggie, S. Jenkins, C.P. Ewels, P. Jemmer, R. Jones, P.R. Briddon, Theory of dislocations in diamond and silicon and their interaction with hydrogen, J. Phys. Condens. Matter 12 (2000) 10263–10270.
[326] L. Thilly, R. Ghisleni, C. Swistak, J. Michler, In situ deformation of micro-objects as a tool to uncover the micro-mechanisms of the brittle-to-ductile transition in semiconductors: the case of indium antimonide, Philos. Mag. 92 (2012) 3315–3325.
[327] L. Pizzagalli, J.L. Demenet, J. Rabier, Theoretical study of pressure effect on the dislocation core properties in semiconductors, Phys. Rev. B 79 (2009) 045203–045209.
[328] O.B.M. Hardouin Duparc, M. Torrent, A new type of periodic boundary condition useful for high-temperature atomistic simulations of grain boundaries: applications in semiconductors, Interface Sci. 2 (1994) 7–16.
[329] L.M. Sandratskii, Noncollinear magnetism in itinerant-electron systems: theory and applications, Adv. Phys. 47 (1998) 91–160.
[330] T. Vegge, J.P. Sethna, S.A. Cheong, K.W. Jacobsen, C.R. Myers, D.C. Ralph, Calculation of quantum tunneling for a spatially extended defect: the dislocation kink in copper has a low effective mass, Phys. Rev. Lett. 86 (2001) 1546–1549.
[331] M.R. Gilbert, P. Schuck, B. Sadigh, J. Marian, Free energy generalization of the Peierls potential in iron, Phys. Rev. Lett. 111 (2013) 095502–095506.
[332] C. Varvenne, G. P. M. Leyson, M. Ghazisaeidi, W. A. Curtin, Solute strengthening of fcc and hcp metals, to appear in Acta Mater. (2016).
[333] G. Seifert, Tight-binding density functional theory: an approximate Kohn-Sham DFT scheme, J. Phys. Chem. A 111 (2007) 5609–5613.
[334] A.C. Van Duin, S. Dasgupta, F. Lorant, W.A. Goddard, ReaxFF: a reactive force field for hydrocarbons, J. Phys. Chem. A 105 (2001) 9396–9409.
[335] J. Yu, S.B. Sinnott, S.R. Phillpot, Charge optimized many-body potential for the Si/SiO2 system, Phys. Rev. B 75 (2007) 085311.
[336] M.J. Noordhoek, T. Liang, Z. Lu, T.R. Shan, S.B. Sinnott, S.R. Phillpot, Charge-optimized many-body (COMB) potential for zirconium, J. Nucl. Mater. 441 (2013) 274–279.
[337] J. Bonneville, B. Escaig, Cross-slipping process and the stress-orientation dependence in pure copper, Acta Metall. 27 (1979) 1477–1486.
[338] Z. Li, R. Picu, Shuffle-glide dislocation transformation in Si, J. Appl. Phys. 113 (2013) 083519.
[339] J.R. Greer, J.T.D. Hosson, Plasticity in small-sized metallic systems: intrinsic versus extrinsic size effect, Prog. Mater. Sci. 56 (2011) 654–724.
[340] J. Rabier, A. Montagne, J.L. Demenet, J. Michler, R. Ghisleni, Silicon micro-pillars: high stress plasticity, Phys. Stat. Sol.(c) 10 (2013) 11–15.